Monthly Notices of the ROYAL ASTRONOMICAL SOCIETY

MNRAS **460,** 3100–3118 (2016) doi:10.1093/mnras/stw1225
Advance Access publication 2016 May 23

Subhalo abundance matching and assembly bias in the EAGLE simulation

Jonás Chaves-Montero,[1]★ Raul E. Angulo,[1] Joop Schaye,[2] Matthieu Schaller,[3] Robert A. Crain,[4]† Michelle Furlong[3] and Tom Theuns[3]

[1]*Centro de Estudios de Física del Cosmos de Aragón, Plaza San Juan 1, Planta-2, E-44001 Teruel, Spain*
[2]*Leiden Observatory, Leiden University, PO Box 9513, NL-2300 RA Leiden, the Netherlands*
[3]*Institute for Computational Cosmology, Department of Physics, University of Durham, South Road, Durham DH1 3LE, UK*
[4]*Astrophysics Research Institute, Liverpool John Moores University, 146 Brownlow Hill, Liverpool L3 5RF, UK*

Accepted 2016 May 19. Received 2016 May 18; in original form 2015 July 7

ABSTRACT

Subhalo abundance matching (SHAM) is a widely used method to connect galaxies with dark matter structures in numerical simulations. SHAM predictions agree remarkably well with observations, yet they still lack strong theoretical support. We examine the performance, implementation, and assumptions of SHAM using the 'Evolution and Assembly of Galaxies and their Environment' (EAGLE) project simulations. We find that $V_{\rm relax}$, the highest value of the circular velocity attained by a subhalo while it satisfies a relaxation criterion, is the subhalo property that correlates most strongly with galaxy stellar mass ($M_{\rm star}$). Using this parameter in SHAM, we retrieve the real-space clustering of EAGLE to within our statistical uncertainties on scales greater than 2 Mpc for galaxies with $8.77 < \log_{10}(M_{\rm star}[{\rm M}_\odot]) < 10.77$. Conversely, clustering is overestimated by 30 per cent on scales below 2 Mpc for galaxies with $8.77 < \log_{10}(M_{\rm star}[{\rm M}_\odot]) < 9.77$ because SHAM slightly overpredicts the fraction of satellites in massive haloes compared to EAGLE. The agreement is even better in redshift space, where the clustering is recovered to within our statistical uncertainties for all masses and separations. Additionally, we analyse the dependence of galaxy clustering on properties other than halo mass, i.e. the assembly bias. We demonstrate assembly bias alters the clustering in EAGLE by 20 per cent and $V_{\rm relax}$ captures its effect to within 15 per cent. We trace small differences in the clustering to the failure of SHAM as typically implemented, i.e. the $M_{\rm star}$ assigned to a subhalo does not depend on (i) its host halo mass, (ii) whether it is a central or a satellite. In EAGLE, we find that these assumptions are not completely satisfied.

Key words: galaxies: evolution – galaxies: formation – galaxies: haloes – dark matter – large-scale structure of Universe.

1 INTRODUCTION

The clustering of galaxies offers an excellent window to explore galaxy formation processes and the fundamental properties of our Universe. On small scales, correlation functions can inform us about the way in which galaxies populate dark matter (DM) haloes and thus about the efficiency of star formation and the importance of environmental effects. On large scales, the clustering of galaxies can be used to constrain cosmological parameters and the law of gravity. On even larger scales, the observed distribution of galaxies is sensitive to the physics of inflation and relativistic effects. By using correlation functions of different orders and at distinct scales, degeneracies among several parameters can be broken, providing even tighter constrains on all the aforementioned quantities.

To extract the information encoded in the clustering of galaxies, we need accurate predictions for a given cosmological scenario and galaxy formation model. However, obtaining the correct galaxy distribution is a difficult task, especially at small scales where besides highly non-linear dynamics, gravitational collapse, mergers, dynamical friction, and tidal stripping; baryonic processes such as star formation, feedback, and ram pressure are at play. Consequently, one needs to resort to numerical simulations to obtain accurate predictions for galaxy clustering (see Kuhlen, Vogelsberger & Angulo 2012, for a review).

Two types of approach can be followed. The first is to simulate the joint evolution of DM and baryons by solving the Poisson and Euler equations coupled with recipes for unresolved physical processes (e.g. star and black hole formation). Although this approach currently yields the most direct predictions for the distribution of galaxies, it is computationally infeasible to simulate large cosmological volumes with adequate resolution for calculating accurately

★ E-mail: jchaves@cefca.es
† Royal Society University Research Fellow.

the galaxy clustering on scales of the order of $100\,h^{-1}$ Mpc. In addition, simulations have only recently begun to produce populations of realistic galaxies (Vogelsberger et al. 2014; Schaye et al. 2015).

The second approach is to simulate only gravitational interactions and to predict the galaxy clustering a posteriori. This is justified by leading theories of galaxy formation, where DM plays the dominant role in determining the places where galaxies form and merge. Gravity-only simulations (a.k.a. DM-only simulations) are computationally less expensive and can thus follow sufficiently large volumes to enable the correct interpretation of observational surveys. This is an important advantage since, for instance, to model galaxy clustering on scales beyond $100\,h^{-1}$ Mpc, it is necessary to perform N-body simulations of volumes in excess of $1\,h^{-3}\,\mathrm{Gpc}^3$ (Angulo et al. 2008). The disadvantage is that the predictions for galaxy clustering are more uncertain because the relation between galaxies and DM haloes is not straightforward.

Subhalo abundance matching (SHAM; e.g. Vale & Ostriker 2004; Conroy, Wechsler & Kravtsov 2006; Shankar et al. 2006) is a widely used method to populate gravity-only simulations with galaxies. The original version of SHAM assumes an injective and monotonic relation between galaxies and self-bound DM structures based on a set of specified properties. SHAM usually links galaxies to DM structures using stellar mass as galaxy property and a measure of subhalo mass, such as circular velocity, as subhalo property. More recent implementations introduce stochasticity into the relation to make the model more realistic (e.g. Behroozi, Conroy & Wechsler 2010; Trujillo-Gomez et al. 2011; Reddick et al. 2013; Zentner, Hearin & van den Bosch 2014). Then, SHAM places each galaxy at the centre-of-potential (COP) of its corresponding subhalo and assumes that each galaxy has the same velocity as the centre-of-mass of its linked subhalo. SHAM thus makes predictions for the clustering of galaxies, but not for any physical properties such as stellar mass, star formation rate, metallicity, etc.

SHAM predictions have been shown to agree remarkably well with observations (e.g. Conroy et al. 2006; Behroozi et al. 2010; Guo et al. 2010; Moster et al. 2010; Wetzel & White 2010; Trujillo-Gomez et al. 2011; Watson, Berlind & Zentner 2012; Nuza et al. 2013; Reddick et al. 2013). For instance, Conroy et al. (2006) showed that SHAM reproduces the observed galaxy clustering over a broad redshift interval ($0 < z < 5$). More recently, Reddick et al. (2013) achieved a simultaneous fit to the clustering and the conditional stellar mass function measured in the Sloan Digital Sky Survey. Simha & Cole (2013) even used this model to constrain cosmological parameters, finding values in good agreement with those obtained from more established methods.

Despite these successes, the comparison with simulations of galaxy formation has not been so encouraging. Weinberg et al. (2008) found that the galaxy clustering predicted by SHAM only agrees with that of a hydrodynamical simulation beyond $1\,h^{-1}$ Mpc. On smaller scales, the differences were of the order of a few. Simha et al. (2012) extended the previous study using two hydrodynamic simulations with different feedback models. They found that the clustering predicted by SHAM exceeded that of their most realistic simulation by more than a factor of 2 on scales below $0.5\,h^{-1}$ Mpc. Finally, in a direct comparison with two semi-analytic models of galaxy formation, Contreras et al. (2015) found that SHAM performs well at some galaxy number densities, but not at others.

It is therefore not clear whether SHAM is able to match the observed galaxy clustering because it makes accurate assumptions (i.e. the physical relation between subhaloes and galaxies) or because some implementations employ free parameters (e.g. a scatter between subhalo and galaxy properties or a cut-off in the fraction of satellite galaxies) that provide enough freedom to become insensitive to them. The importance of the information being decoded, added to the fact that the amount and accuracy of clustering data will increase dramatically over the next decade due to the emergence of wide-field galaxy surveys (e.g. DES, HETDEX, eBOSS, JPAS, DESI, *EUCLID*, and LSST), makes it crucial to critically test the assumptions underlying SHAM.

In this paper, we will employ the state-of-the-art hydrodynamical simulations 'Evolution and Assembly of Galaxies and their Environment' (EAGLE; Crain et al. 2015; Schaye et al. 2015) to study the SHAM technique in detail. Our objectives are threefold, (i) to seek the most accurate implementation of SHAM, (ii) to directly test the underlying assumptions, and (iii) to assert how accurately SHAM can predict galaxy clustering.

We will propose $V_{\rm relax}$, defined as the maximum of the circular velocity of a DM structure along its entire history while it fulfils a relaxation criterion, as the best subhalo property with which to perform SHAM. We will show that this definition captures the best qualities of previously proposed implementations while mitigating their disadvantages and reducing the number of problematic cases. As a consequence, $V_{\rm relax}$ shows the strongest correlation with the simulated stellar mass of EAGLE galaxies.

We will show that SHAM is able to reproduce the clustering properties of stellar mass selected galaxies in the EAGLE simulation (which successfully reproduces many properties of observed low-z galaxies). For the stellar mass range investigated ($10^{8.77} < M_{\rm star}[\mathrm{M}_\odot] < 10^{10.77}$), the agreement is better than 10 per cent on scales greater than 2 Mpc, and better than 30 per cent on smaller scales. The agreement is particularly good for massive galaxies and in redshift space, for which we do not find statistically significant difference between the clustering predicted by SHAM and EAGLE. This is remarkable given that we explore almost two orders of magnitude in spatial scale and four in clustering amplitude.

Additionally, we will pay attention to the so-called assembly bias: the dependence of the clustering of DM haloes on properties other than mass (Gao, Springel & White 2005; Wechsler et al. 2006; Zhu et al. 2006; Croton, Gao & White 2007; Gao & White 2007; Dalal et al. 2008; Li, Mo & Gao 2008; Zu et al. 2008; Lacerna & Padilla 2011, 2012; Lacerna et al. 2014; Zentner et al. 2014; Hearin, Watson & van den Bosch 2015). We will show that assembly bias is present in both EAGLE and SHAM galaxies, increasing the clustering amplitude by 20 per cent on scales from 2 to 11 Mpc. To our knowledge, this is the first detection of assembly bias in a hydrodynamical simulation. This result supports the idea that halo occupation distribution (HOD) models (e.g. Peacock & Smith 2000; Seljak 2000; Scoccimarro et al. 2001), which are a phenomenological parametrization for the number of galaxies hosted by haloes of a given mass, introduce bias in the calculation of galaxy clustering when they assume that halo occupation is a function only of halo mass.

Finally, we will track the small residual differences in the clustering of SHAM and EAGLE galaxies to the failure of a key assumption of SHAM (as commonly implemented): for the same $V_{\rm relax}$, central and satellite subhaloes host the same galaxies independently of their host halo mass. We will find that this supposition is broken due to the influence of the environment and the star formation that satellite galaxies experience after having been accreted. Both effects correlate with the mass of the DM host, which suggests that future SHAM implementations that employ both host halo mass and $V_{\rm relax}$ could yield even more accurate predictions for the clustering signal.

Our paper is organized as follows. In Section 2 we describe the simulations, halo and galaxy catalogues, and merger trees that we

use. In Section 3 we discuss different implementations of SHAM and introduce $V_{\rm relax}$, a new proxy for stellar mass. In Section 4 we analyse the accuracy with which SHAM can predict the galaxy satellite fraction, host halo mass, clustering, and assembly bias. We discuss the limitations of SHAM in Section 5. We conclude and summarize our most important results in Section 6.

2 NUMERICAL SIMULATIONS

In this section, we provide details of the main data sets that we employ. This includes a brief description of the numerical simulations, halo and galaxy catalogues, merger trees, and of a technique to identify the same structures in our hydrodynamical and gravity-only simulations.

2.1 The EAGLE suite

The simulations we analyse in this paper belong to the EAGLE project (Crain et al. 2015; Schaye et al. 2015) conducted by the Virgo consortium. EAGLE is a suite of high-resolution hydrodynamical simulations aimed at understanding the formation of galaxies in a cosmological volume. The runs employed a pressure-entropy variant (Hopkins 2013) of the Tree-PM smoothed particle hydrodynamics code GADGET3 (Springel 2005), the time step limiters of Durier & Dalla Vecchia (2012), and implement state-of-the-art subgrid physics (as described by Schaye et al. 2015), including metal-dependent radiative cooling and photoheating (Wiersma, Schaye & Smith 2009a), chemodynamics (Wiersma et al. 2009b), gas accretion on to supermassive black holes (Rosas-Guevara et al. 2013), star formation (Schaye & Dalla Vecchia 2008), stellar feedback (Dalla Vecchia & Schaye 2012), and AGN feedback.

The EAGLE suite includes runs with different physical prescriptions, resolutions, and volumes. Here, we study the largest simulation, which follows 1504^3 gas particles and the same number of DM particles inside a periodic box with a side length of 100 Mpc. The large volume and high resolution of this simulation are essential for a careful analysis of SHAM. The cosmological parameters used in EAGLE are those preferred by the analysis of *Planck* data (Table 1). This implies a gas particle mass equal to $1.81 \times 10^6\,{\rm M}_\odot$ and a DM particle mass equal to $9.70 \times 10^6\,{\rm M}_\odot$. We highlight that EAGLE is well suited to this study because it was calibrated to reproduce the galaxy stellar mass function at $z \sim 0$. The agreement with observations is especially good over the mass range that we will analyse here (fig. 4 of Schaye et al. 2015).

The 100 Mpc box was resimulated including only gravitational interactions and sampling the density field with 1504^3 particles of mass $1.15 \times 10^7\,{\rm M}_\odot$. Hereafter, we refer to this simulation and its hydrodynamical counterpart as DMO and EAGLE, respectively. The cosmological and some of the numerical parameters employed in these simulations are provided in Table 1.

Table 1. EAGLE/DMO cosmological and numerical parameters. The cosmological parameter values are taken from Planck Collaboration I (2014) and Planck Collaboration XVI (2014).

Parameter	EAGLE/DMO
$\Omega_{\rm m}$	0.307
Ω_Λ	0.693
$\Omega_{\rm b}$	0.048 25
H_0(km s^{-1} Mpc^{-1})	67.77
σ_8	0.8288
$n_{\rm s}$	0.9611
Max. proper softening (kpc)	0.70
Num. of baryonic particles	1504^3/–
Num. of DM particles	1504^3/1504^3
Initial baryonic particle mass (10^7 M$_\odot$)	0.181/–
DM particle mass (10^7 M$_\odot$)	0.970/1.150

Notes. $\Omega_{\rm m}$, Ω_Λ, and $\Omega_{\rm b}$ are the densities of matter, dark energy, and baryonic matter in units of the critical density at redshift zero. H_0 is the present-day Hubble expansion rate, σ_8 is the linear fluctuation amplitude at 8 h^{-1} Mpc, and $n_{\rm s}$ is the scalar spectral index.

2.2 Catalogues and mergers trees

In each simulation, haloes were identified using only DM particles and a standard friends-of-friends (FoF) group-finder with a linking parameter $b = 0.2$ (Davis et al. 1985). Gas and star particles are assigned to the same FoF halo as their closest DM particle. For each FoF halo we compute a spherical-overdensity mass, M_{200}, defined as the mass inside a sphere with mean density equal to 200 times the critical density of the Universe, $\rho_{\rm crit}(z)$;

$$M_{200} = \frac{4\pi}{3} 200\, \rho_{\rm crit} r_{200}^3, \tag{1}$$

where r_{200} is the radius of the halo, $\rho_{\rm crit}(z) = \frac{3\,H^2(z)}{8\pi G}$, G is the gravitational constant, and $H(z)$ is the value of the Hubble parameter $H(z) = H_0\sqrt{\Omega_{\rm m}(1+z)^3 + \Omega_\Lambda}$.

Self-bound structures inside FoF haloes, termed subhaloes, were identified using all particle types and the SUBFIND algorithm (Springel et al. 2001; Dolag et al. 2009). Hereafter, we will refer to the subhalo located at the potential minimum of a given FoF halo as the 'central', to any other structures as 'satellites', and to subhaloes with more than one star particle as EAGLE 'galaxies'.

The position of each galaxy is assumed to be that of the particle situated at the minimum of the gravitational potential of the respective subhalo. The galaxy velocity is assumed to be that of the centre of mass of the subhalo.[1] The stellar mass, $M_{\rm star}$, is the total mass of all star particles linked to a given EAGLE galaxy. The gas mass ($M_{\rm gas}$) and the DM mass ($M_{\rm DM}$) are computed in the same manner but using gas particles or DM particles, respectively. We verified that our results are insensitive to the exact definition of $M_{\rm star}$: we repeated our analysis defining $M_{\rm star}$ as the mass inside a sphere of 20, 30, 40, 50, 70, or 100 kpc radius. We found that different mass definitions only produces sub-per cent differences in the galaxy clustering.

We employ 'merger trees' to follow the evolution of haloes and subhaloes, their mass growth, tidal stripping, mergers, as well as transient effects in their properties. Our trees were built using the algorithm described in Jiang et al. (2014), employing 201 snapshots for DMO and 29 snapshots for EAGLE. In both simulations the output times were approximately equally spaced in $\log(a)$ for $a > 0.2$, where a is the cosmic scalefactor.

Finally, we note that to avoid problems related to subhalo fragmentation and spurious structures, we remove from our analysis satellites without resolved progenitors.

[1] We checked that the mean difference between the bulk velocity of DM particles and star particles in the inner 30 kpc for the subhaloes with $8.77 < M_{\rm star}[{\rm M}_\odot] < 10.77$ is smaller than 10 km s^{-1}.

Table 2. Number of central and satellite EAGLE galaxies for four stellar mass bins. In parentheses we provide the percentage of EAGLE galaxies with a counterpart in DMO.

	EAGLE	
$\log_{10}(M_{\rm star}[M_\odot])$	Central	Satellites
8.77–9.27	3954 (92 per cent)	3475 (68 per cent)
9.27–9.77	2550 (92 per cent)	2068 (74 per cent)
9.77–10.27	1551 (94 per cent)	1247 (76 per cent)
10.27–10.77	968 (92 per cent)	652 (80 per cent)

2.3 EAGLE and DMO cross-match

EAGLE and DMO share the same initial conditions, so we expect roughly the same non-linear objects to form in both simulations. This is a powerful feature: it enables us to identify the EAGLE galaxy that a given DMO subhalo is expected to host, and thus, to probe directly the assumptions of SHAM.

In practice, we link DMO subhaloes to EAGLE galaxies following the process described by Schaller et al. (2015); see also Velliscig et al. (2014). For every subhalo in EAGLE we select the 50 most-bound DM particles. If we find a subhalo in DMO which shares at least half of them, the link is made. We confirm the link if, repeating the same process starting from each DMO subhalo, we identify the same pair. We only search the pairs with more than 174 DM particles in each simulation, which corresponds to a minimum halo mass of 2×10^9 M$_\odot$ in DMO. This procedure yields a catalogue of 13 687 galaxies with $10^{8.77} < M_{\rm star}[{\rm M}_\odot] < 10^{10.77}$.

In Table 2 we list the fraction of successfully matched centrals and satellites, for four stellar mass bins. Overall, the match is successful for more than 90 per cent of centrals in EAGLE, independently of their mass. The success rate drops to 68–80 per cent for satellites, with low-mass satellites showing the lowest percentage. This is a consequence of the finite mass resolution of the simulations (see also Appendix A), the mass-loss due to interactions with the host halo, small differences in the timing at which mergers happen, and the high-density environment in which they reside.

3 SUBHALO ABUNDANCE MATCHING

In this section, we discuss different SHAM flavours and their implementation in DMO.

3.1 SHAM flavours

The main assumption of SHAM is that there is a one-to-one relation between a property of a DM subhalo and a property of the galaxy that it hosts. The galaxy property is usually taken to be the stellar mass (or *K*-band luminosity), since this is expected to be tightly correlated with the DM content of the host halo (contrary to e.g. the star formation rate, which could be more stochastic). The subhalo property should capture the time-integrated mass of gas available to fuel star formation, but there is no consensus as to what the most adequate subhalo property is.[2]

[2] Properties used in the literature include $M_{\rm DM}$ (Vale & Ostriker 2004; Shankar et al. 2006), maximum circular velocity at present for centrals and at infall for satellites (Conroy et al. 2006), virial mass for centrals and mass at infall for satellites (Behroozi et al. 2010; Wetzel & White 2010), virial mass for centrals and the highest mass along the merger history for satellites (Moster et al. 2010), and highest circular velocity along the merger history (Trujillo-Gomez et al. 2011; Nuza et al. 2013, see Reddick et al. 2013 for a detailed comparison between the previous properties).

A commonly used property in SHAM is the maximum of the radial circular velocity profile (which can be regarded as a measure of the depth of the potential well of a subhalo) defined at a suitable time:

$$V_{\rm circ}(z) \equiv \max[\sqrt{GM(z, < r)/r}], \quad (2)$$

where $M(<r)$ is the mass enclosed inside a radius r.

There are several reasons to prefer circular velocity over halo mass in SHAM: (i) it is typically reached at one-tenth of the halo radius, so it is a better characterization of the scales that we expect to affect the galaxy most directly; (ii) it is less sensitive to the mass stripping that a halo/subhalo experiences after it has been accreted by a larger object (Hayashi et al. 2003; Kravtsov, Gnedin & Klypin 2004; Nagai & Kravtsov 2005; Peñarrubia, McConnachie & Navarro 2008); (iii) it does not depend on the definition of halo/subhalo mass.

However, the $V_{\rm circ}(z)$ of DM objects are complicated functions, which can display non-monotonic behaviour in time, with transient peaks and dips, and that are subject to environmental and numerical effects. This is illustrated by Fig. 1, which shows examples of the evolution of the circular velocity for two central (left-hand panel) and two satellite (right-hand panel) subhaloes in DMO. These subhaloes are selected to illustrate the evolution of the maximum circular velocity in typical centrals and satellites. We can see that there is no obvious time at which $V_{\rm circ}(z)$ should be computed for an accurate SHAM.

We will implement four 'flavours' of SHAM, each using $V_{\rm circ}(z)$ defined at a different time: $V_{\rm max}$, $V_{\rm peak}$, $V_{\rm infall}$, and $V_{\rm relax}$ (each marked by horizontal lines and arrows of a different colour in Fig. 1). The first three flavours have been used previously in the literature, whereas the fourth is first used in this work. We discuss the four SHAM flavours next.

(1) $V_{\rm max}$ is the maximum circular velocity of a subhalo at the present time, $V_{\rm circ}(z = 0)$.

(2) $V_{\rm infall}$ is the maximum circular velocity at the last time a subhalo was identified as a central.

(3) $V_{\rm peak}$ is the maximum circular velocity that a subhalo has reached.

(4) $V_{\rm relax}$ is the maximum circular velocity that a subhalo has reached during the periods in which it satisfied a relaxation criterion. The criterion we use is $\Delta t_{\rm form} > t_{\rm cross}$, following a similar approach to Ludlow et al. (2012). The motivation is that after a major merger, DM haloes typically need of the order of one crossing time ($t_{\rm cross} = 2\, r_{200}/V_{200} = 0.2/H(z)$) to return to equilibrium. Thus, we define $\Delta t_{\rm form}$ as the look-back time from a given redshift $z_{\rm i}$ to the redshift where the main progenitor of a subhalo reached 3/4 of the subhalo mass at $z_{\rm i}$ (we tested other definitions for the formation time, from 4/5 to 1/2, finding roughly the same results). The periods during which this condition is satisfied are shown as blue shaded regions in Fig. 1. We can compute $V_{\rm relax}$ for more than the 99 per cent of the subhaloes in DMO and we remove the subhaloes where $V_{\rm relax}$ cannot be calculated. We cannot compute $V_{\rm relax}$ for the full sample because this quantity is not defined for subhaloes younger than one crossing time.

Although $V_{\rm circ}$ should generally not be affected by the stripping of the outer layers of a halo, in the right-hand panel of Fig. 1 we can see that it does still evolve for satellites. The decrease in $V_{\rm circ}(z)$

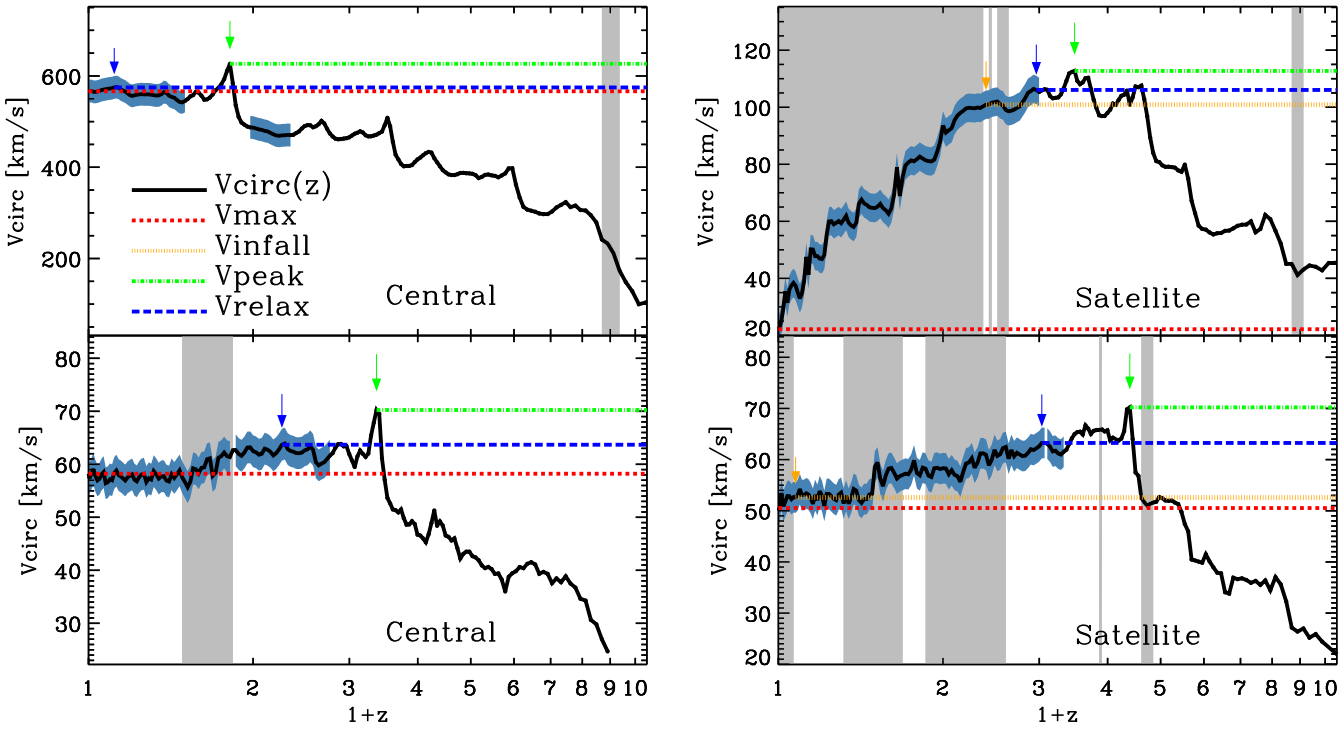

Figure 1. Evolution of the maximum circular velocity of two central (left-hand panel) and two satellite (right-hand panel) subhaloes in DMO. The black solid lines show the circular velocity, the grey coloured areas the periods during which the subhaloes are satellites, and the blue coloured regions the intervals during which the subhaloes satisfy our relaxation criterion. Horizontal lines highlight the circular velocity at $z = 0$ ($V_{\rm max}$, red dashed line), the circular velocity at the last infall for satellites and $V_{\rm max}$ for centrals ($V_{\rm infall}$, orange dotted line), the maximum circular velocity that a subhalo has had ($V_{\rm peak}$, green dot–dashed line), and the maximum circular velocity that a subhalo has reached while it satisfied our relaxation criterion ($V_{\rm relax}$, blue long dashed line).

after infall is in large part due to tidal heating, a process which reduces the density in the inner regions of the satellites (Gnedin 2003; Hayashi et al. 2003; Kravtsov et al. 2004). The tidal heating is related to the position of a subhalo inside its host halo, being maximum at pericentric passages. We can see an extreme case of tidal interactions in the top-right panel, where this subhalo has lost more than 99 per cent of its mass since it became a satellite. After the last infall at $1 + z \sim 2.3$ (grey shaded region), the value of $V_{\rm circ}$ decreased by about 80 per cent in a series of steps ($z \sim 1, 0.5, 0.3, 0.1, 0.05,$ and 0), which indeed coincide with pericentric passages. This implies that satellite galaxies have lower values of $V_{\rm max}$ than central galaxies of the same stellar mass. Thus, a $V_{\rm max}$-based SHAM will underestimate the fraction of satellites.

Tidal heating and stripping affect not only satellites but also 'backsplash satellites', i.e. centrals at $z = 0$ which were satellites in the past, reducing their circular velocity while they were inside a larger halo. An example of this process is shown in the bottom-left panel of Fig. 1, where the circular velocity of this subhalo was reduced by about 7 per cent in the period during which it was a satellite (while the mass was reduced by 50 per cent).

$V_{\rm infall}$ is less affected by these problems. Unfortunately, this parameter also underestimates $V_{\rm circ}$ for satellites because tidal heating starts to act even before a satellite is accreted by its future host halo (Kravtsov et al. 2004; Wetzel et al. 2013, 2014). This can be seen in the top (bottom) right-hand panel of Fig. 1, where the value of $V_{\rm circ}$ starts to decrease at $1 + z \sim 3.4$ ($1 + z \sim 4.4$) while the subhalo is accreted at $1 + z \sim 2.4$ ($1 + z \sim 1.2$).

Additionally, there are new problems associated with $V_{\rm infall}$. The first concerns satellite–satellite mergers (Angulo et al. 2009; Wetzel, Cohn & White 2009), which should increase the mass of stars in a satellite but this is not captured by $V_{\rm infall}$. The second is related to the definition of $V_{\rm infall}$; it is not clear whether we should consider $V_{\rm infall}$ as the circular velocity at the last infall or at previous accretion events. We can see in the bottom-right panel of Fig. 1 a satellite which has undergone several alternating central/satellite periods, decreasing in total its circular velocity by 20 per cent and its mass by 70 per cent.

An alternative solution is provided by $V_{\rm peak}$ since it can capture all episodes during which the subhalo grows, and it is not affected by a reduction of $V_{\rm circ}$ due to environmental effects. However, this definition similarly has its own problems. During periods of rapid mass accretion, DM haloes are usually out of equilibrium (Neto et al. 2007). In particular, during major mergers the concentration can be artificially high (this is a maximum compression phase of halo formation), which temporarily increases the value of $V_{\rm circ}$ (e.g. Ludlow et al. 2012; Behroozi et al. 2014). This effect is responsible for the peaks seen in all four panels of Fig. 1. Although at any given time it is rare to find a halo in this phase, the value of $V_{\rm peak}$ will likely be assigned during one of these phases, and will thus overestimate the depth of the potential well. In addition, this effect makes the predictions of $V_{\rm peak}$ dependent on the number and intervals of the output times of a given simulation.

Here we propose a new measure, $V_{\rm relax}$, designed to overcome the problems of $V_{\rm max}$, $V_{\rm infall}$, and $V_{\rm peak}$. It is marked by arrows and horizontal lines of blue colour in Fig. 1. $V_{\rm relax}$ is insensitive to tidal heating, transient peaks, and consistently defined for centrals, satellites, and backsplash satellites. We emphasize that it is desirable to eliminate the aforementioned problems because they represent changes in $V_{\rm circ}$ which are not expected to correlate with the growth history of $M_{\rm star}$, and will thus add extra noise to SHAM.

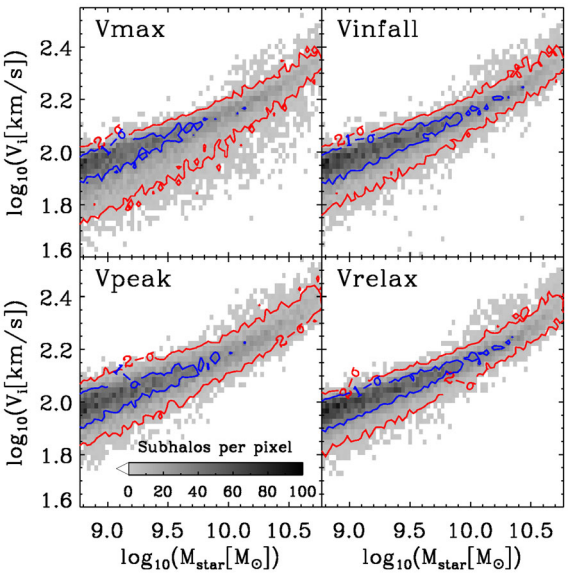

Figure 2. Relation between $M_{\rm star}$ of EAGLE galaxies and SHAM flavours for the corresponding DMO subhaloes. The grey-scale represents the number of subhaloes per pixel, which ranges from 1 (light grey) to 100 (black). Blue and red contours mark the regions containing 68 and 95 per cent of the distribution, respectively.

We now take a first look at the performance of each SHAM flavour. Fig. 2 shows the relation between each of the four properties described above for DMO subhaloes, as indicated by the legend, and $M_{\rm star}$ of their galaxy counterpart in EAGLE (see Section 2.3). All panels show a tight correlation, which supports the main assumption of SHAM, that the relation between stellar mass and SHAM parameters should be monotonic. However, the scatter in the relation is different in each panel because of the effects discussed in this section: $V_{\rm max}$ shows the largest and $V_{\rm relax}$ the smallest dispersion. In the next sections we will quantify the performance of each SHAM flavour in detail.

3.2 Implementation

The first step to implement the four flavours of SHAM is to compute $P(\log_{10}{\rm M_{star}}|\log_{10}V_i)$: the probability that a subhalo hosts a galaxy of mass $M_{\rm star}$ given a certain value of the SHAM flavour V_i. We compute this quantity as follows.

(1) We select subhalo–galaxy pairs from the matched catalogues (see Section 2.3) with $\log_{10}M_{\rm star}[{\rm M}_\odot] > 7$ and divide them according to $\log_{10}V_i$ in bins of 0.05 dex. We discard bins with fewer than 100 objects.

(2) For each $\log_{10}V_i$ bin, we compute the distribution of $\log_{10}M_{\rm star}$ and fit it by a Gaussian function, $G \sim \exp(-0.5(\log_{10}M_{\rm star} - \mu)^2/(\sigma)^2)$, where μ is the mean and σ the dispersion.

(3) We fit a linear function, $\sigma = a + b\log_{10}V_i$, to $\sigma(\log_{10}V_i)$ and an arctangent, $\mu = a + b\tan^{-1}(c + d\log_{10}V_i)$, to $\mu(\log_{10}V_i)$. The values of the best-fitting parameters are given in Table 3 and the quality of the fit can be judged from Fig. 3.

(4) Using these functions, we model $P(\log_{10}{\rm M_{star}}|\log_{10}V_i)$ as $G[\mu(\log_{10}V_i), \sigma(\log_{10}V_i)]$.

Our second step is to assign a value of $M_{\rm star}$ to every subhalo in DMO (not only those with an EAGLE counterpart) by randomly sampling $P(\log_{10}{\rm M_{star}}|\log_{10}V_i)$. This creates a catalogue that captures the appropriate stochastic relation between $M_{\rm star}$ and the parameter V_i. If the relation for EAGLE galaxies were also stochastic with respect to the underlying density field, then we would expect these catalogues to have the same clustering properties as EAGLE.

We note we have verified that the resulting stellar mass function agrees closely with that of the EAGLE simulation. However, to ensure *identical* mass functions and thus to make subsequent comparisons more direct, we assign to each SHAM galaxy the value of $M_{\rm star}$ of the EAGLE galaxy at the same rank order position. Hereafter, we will refer generically to the galaxy catalogues created in this way as 'SHAM galaxies' and specifically to the galaxy catalogues generated by a particular SHAM parameter as 'V_i galaxies'.

We compute 100 realizations of SHAM for every flavour using different random seeds. The results presented in the following sections are the mean of all the realizations and the errors the standard deviation.

Table 3. Parameters of the functions that fit the mean, μ, and standard deviation, σ, of the model for $P(\log_{10}M_{\rm star}[{\rm M}_\odot]|\log_{10}V_i[{\rm km\,s^{-1}}])$. The unit of V_i is ${\rm km\,s^{-1}}$.

	$\sigma = a + b\log_{10}V_i$		$\mu = a + b\tan^{-1}(c + d\log_{10}V_i)$			
	a	b	a	b	c	d
$V_{\rm max}$	0.60	−0.20	7.03	5.52	−1.84	1.12
$V_{\rm infall}$	0.53	−0.16	7.01	5.52	−1.84	1.12
$V_{\rm peak}$	0.55	−0.16	7.70	5.42	−1.89	1.05
$V_{\rm relax}$	0.59	−0.20	7.14	5.55	−1.86	1.10

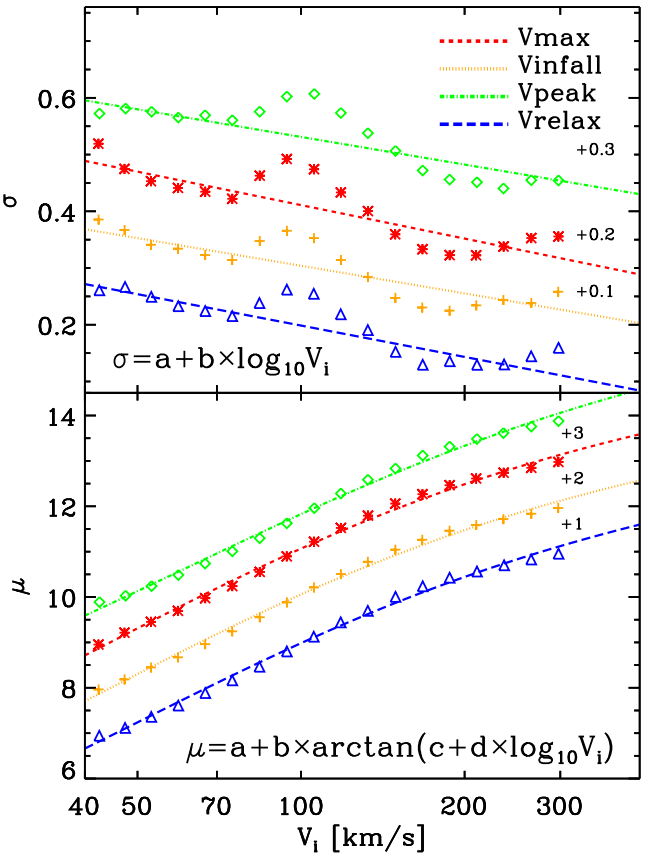

Figure 3. Standard deviation (top panel) and mean (bottom panel) of the Gaussians used to fit PDFs for $\log_{10}M_{\rm star}[{\rm M}_\odot]$. For clarity, we have shifted the σ (μ) of $V_{\rm max}$, $V_{\rm infall}$, and $V_{\rm peak}$ by +0.3, +0.2, and +0.1 (+3, +2, and +1), respectively. The best-fitting functions are shown by coloured lines, and the values of the respective parameters are given in Table 3.

4 RESULTS

In this section, we test how well SHAM reproduces different properties of EAGLE galaxies. In particular, we will explore the predicted stellar mass of individual subhaloes (Section 4.1), the HOD (Section 4.2.1), the number density profiles inside haloes (Section 4.2.2), the clustering in real and redshift space (Sections 4.3.1 and 4.3.2), and the assembly bias (Section 4.3.3).

We present results for four bins in stellar mass, as indicated in Table 2. This range was chosen to include only well-sampled and well-resolved galaxies (comprised of more than 230 star particles) and bins with enough galaxies to allow statistically significant analyses (more than 1600 galaxies).

4.1 Correlation between $M_{\rm star}$ and V_i

In Section 3 we discussed that in some cases $V_{\rm max}$, $V_{\rm infall}$, and $V_{\rm peak}$ are unintentionally affected by physical and numerical effects, which degrades the performance of SHAM. We also argued that $V_{\rm relax}$ does not present any obvious problem and thus we expected it to be the SHAM flavour that correlates most strongly with $M_{\rm star}$. This was qualitatively supported by Fig. 2. We start this section by quantifying these statements using the Spearman rank correlation coefficient between the $M_{\rm star}$ of EAGLE galaxies and the SHAM flavours of DMO subhaloes.

The Spearman coefficient measures the statistical dependence between two quantities and is defined as the Pearson correlation coefficient between the ranks of sorted variables. A value of unity implies a perfect correlation, which in our case means that the stellar mass of a galaxy is completely determined by its SHAM parameter, i.e. the relation is monotonic and thus without scatter. A value close to zero means that the relation between the SHAM parameter and $M_{\rm star}$ is essentially random.

In Fig. 4, we show the Spearman coefficient for the correlation between $M_{\rm star}$ and each of our four SHAM parameters. We divide our sample into three groups: (i) present-day central subhaloes that have been centrals for their entire merger history except for at most four snapshots (centrals, left-hand panel), (ii) present-day central subhaloes that have been satellites more than four snapshots in the past (backsplash satellites, central panel), and (iii) present-day satellites (satellites, right-hand panel).

In general, we find that the correlation increases with $M_{\rm star}$, that it is stronger for centrals than for satellites, and that $V_{\rm relax}$ displays the strongest correlation with $M_{\rm star}$. Regarding the different SHAM flavours, we find that (i) for centrals $V_{\rm peak}$ produces the weakest correlation, (ii) for satellites $V_{\rm max}$ shows the weakest correlations, and (iii) $V_{\rm infall}$ and $V_{\rm relax}$ consistently display the best performance, with $V_{\rm relax}$ showing a slight improvement over $V_{\rm infall}$ for satellites.

Our results can be understood from the discussion in Section 2. For centrals, $V_{\rm max}$ and $V_{\rm infall}$ are identical by construction and they are close to the value of $V_{\rm relax}$ because $V_{\rm circ}$ tends to increase with decreasing redshift for centrals. On the other hand, $V_{\rm peak}$ is usually established while $V_{\rm circ}$ is temporarily enhanced as a result of merger events. For backsplash satellites, $V_{\rm max}$ and $V_{\rm infall}$ are also identical by construction, but, unlike $V_{\rm relax}$, they are insensitive to their more complicated history, which explains their weaker correlation with $M_{\rm star}$.

Finally, satellites display the weakest correlations, with $V_{\rm max}$ presenting the lowest correlation coefficient. This is because $V_{\rm circ}$ decreases soon after infall, whereas the stellar mass can still grow until the gas is completely exhausted (although tidal forces may strip stars). $V_{\rm infall}$ alleviates this problem but the interaction between the satellites and their host haloes starts before the satellites reach the virial radii of their host haloes (Hayashi et al. 2003; Bahé et al. 2013). Because of this, $V_{\rm relax}$ better captures the expected evolution in $M_{\rm star}$. Lastly, $V_{\rm peak}$ is still affected by the out-of-equilibrium artefacts discussed above.

In sections Sections 4.2 and 4.3, we will investigate how the different correlations impact the predictions for the clustering of EAGLE galaxies.

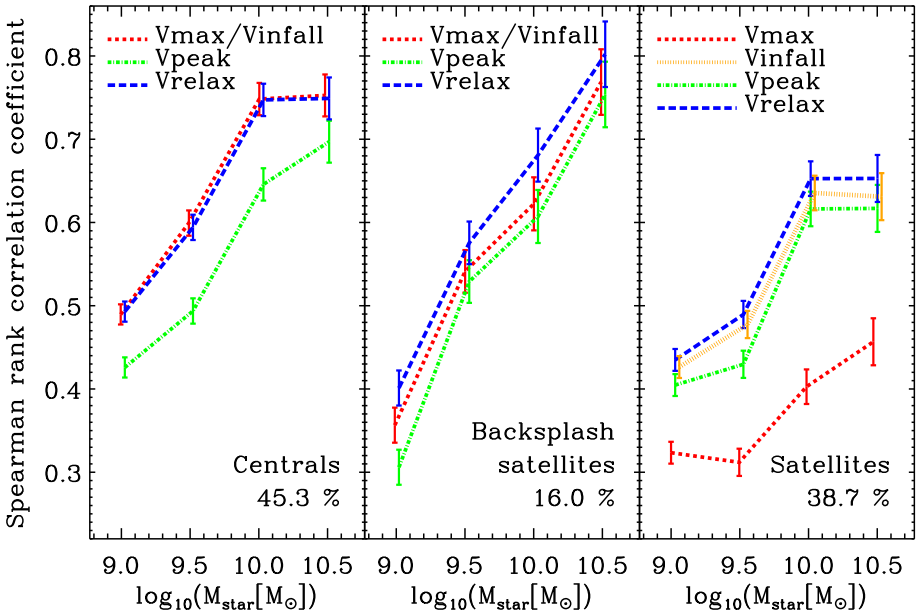

Figure 4. The Spearman rank correlation coefficient between the $M_{\rm star}$ of EAGLE galaxies and each of four parameters used to perform SHAM. The subhaloes are divided into three categories: centrals (left-hand panel), backsplash satellites (central panel), and satellites (right-hand panel), see the main text for more details. The fraction of objects in each category is given in the legend. The red (orange) points are displaced horizontally by −0.03 (+0.03) dex for clarity.

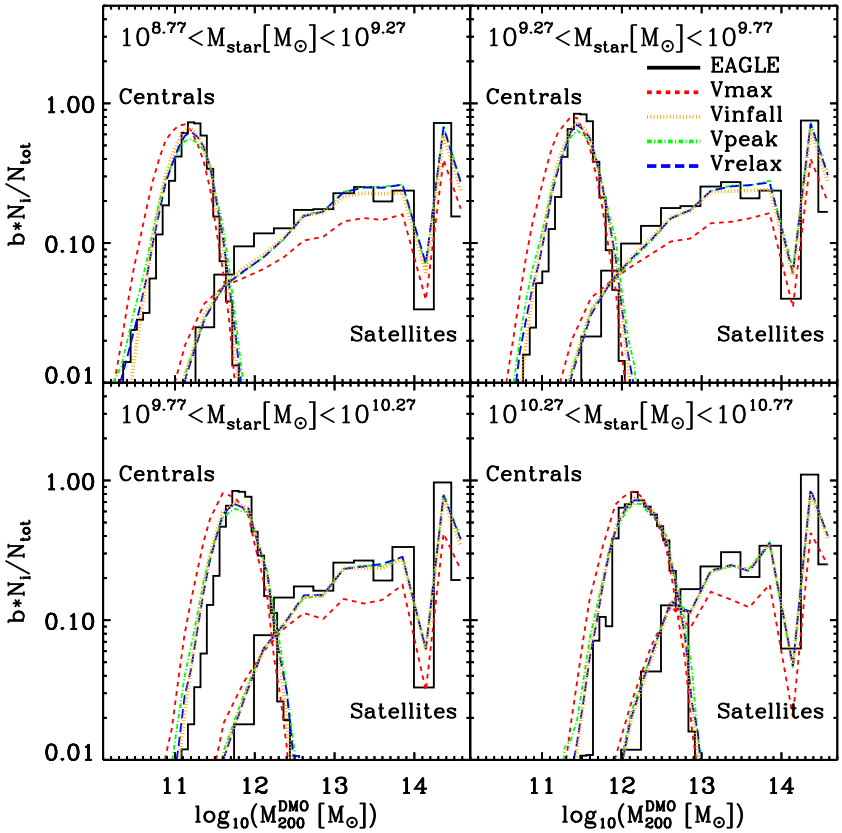

Figure 5. The distribution of host halo masses, M_{200}, for SHAM and EAGLE galaxies in different $M_{\rm star}$ bins. Histograms show the results for EAGLE galaxies and coloured lines for different SHAM flavours, as detailed in Section 3.2. The left (right) curves display the number N_i of centrals (satellites) in haloes of a given mass multiplied by the linear bias b and normalized by the total number of subhaloes $N_{\rm tot}$. Therefore, the y-axis reflects the relative contribution of galaxies in different host halo mass bins to the large-scale correlation function. Note that for EAGLE galaxies we employ the M_{200} of the DMO counterpart, which makes our comparison less dependent on the baryonic processes which might alter the mass of the host halo.

4.2 The properties of SHAM galaxies

To predict the correct galaxy clustering, SHAM has to associate galaxies with the correct subhaloes, to allocate the right proportion of centrals and satellites, and to place galaxies following the correct radial distribution. Therefore, before presenting our results regarding the clustering, we will explore these ingredients separately.

4.2.1 Halo occupation distribution

The panels of Fig. 5 show the distribution of host halo masses for centrals and satellites in different $M_{\rm star}$ bins. The left (right) curves display the number of centrals (satellites) in haloes of a given mass multiplied by the linear bias[3] expected for haloes of that mass and normalized by the total number of subhaloes. The quantity plotted can be interpreted as the relative contribution to the large-scale clustering from galaxies hosted by haloes of different mass. In each panel, the histogram presents the results for EAGLE galaxies and the coloured lines the results of the SHAM implementations detailed in Section 3.2. For EAGLE galaxies we employ the M_{200} of their host halo DMO counterpart, which makes this plot less sensitive to baryonic effects that might systematically change the mass of DM haloes. For the 5.1 per cent of EAGLE galaxies hosted by a halo without DMO counterpart, we multiply M_{200} by $f_{\rm DM} = 1 - (\Omega_{\rm b}/\Omega_{\rm m}) = 0.843$. This is the average difference in M_{200} between the hydrodynamic and gravity-only EAGLE simulations, as reported by Schaller et al. (2015).

First, we see that using $V_{\rm max}$ as SHAM parameter results in shifted M_{200} distributions and an underprediction, of about 30 per cent, of the number of satellites for all $M_{\rm star}$ bins. This is a consequence of the reduction of $V_{\rm max}$ for satellites after being accreted, which introduces centrals hosted by lower mass haloes into the SHAM sample.

The distribution of EAGLE galaxies is closely reproduced by the other SHAM implementations, for all stellar mass bins. The distributions for central galaxies have almost identical shapes and peak at roughly the same host halo mass. Note, however, that compared to $V_{\rm infall}$ and $V_{\rm relax}$, $V_{\rm peak}$ yields systematically broader distributions for centrals. This is consistent with the differences in the correlation coefficient shown in the left-hand panel of Fig. 4.

Additionally, the $V_{\rm infall}$, $V_{\rm peak}$, and $V_{\rm relax}$ satellite fractions agree to within $\sim$5 per cent with those in EAGLE, although they are systematically lower, as shown in Table 4. However, for the two lowest stellar mass bins, there is a slight overestimate of the number of satellites in haloes of mass $M_{200} > 10^{13}\,{\rm M}_\odot$, and a somewhat larger underestimate for haloes of mass $M_{200} < 10^{13}\,{\rm M}_\odot$, as Table 5 shows. Since the difference is greater for the high-mass haloes, the overall satellite fraction is underestimated. We will

[3] We calculate the linear bias as $b = 1 + \frac{\nu^2 - 1}{\delta_{\rm c}}$ (Mo & White 1996), where $\delta_{\rm c} \approx 1.69$ is the critical linear overdensity at collapse and $\nu = \delta_{\rm c}/\sigma(M, z)$ is the dimensionless amplitude of fluctuations which produces haloes of mass M at redshift z.

Table 4. Satellite fraction for EAGLE and SHAM galaxies using V_{max}, V_{infall}, V_{peak}, and V_{relax}.

$\log_{10}(M_{star}[M_\odot])$	V_{max}	V_{infall}	V_{peak}	V_{relax}	EAGLE
			Satellite fraction		
8.77–9.27	0.32	0.43	0.46	0.45	0.47
9.27–9.77	0.30	0.42	0.44	0.43	0.45
9.77–10.27	0.28	0.40	0.41	0.41	0.44
10.27–10.77	0.25	0.37	0.38	0.37	0.40

Table 5. Number of satellites as a function of M_{star} and M_{200} for EAGLE and SHAM galaxies using V_{relax}.

$\log_{10}(M_{star}[M_\odot])$	$\log_{10}(M_{200}[M_\odot])$	EAGLE	V_{relax}
		N. of satellites	
8.77–9.27	11.6–12.6	1060	780
	12.6–13.6	1274	1328
	13.6–14.6	945	1057
9.27–9.77	11.6–12.6	584	444
	12.6–13.6	834	838
	13.6–14.6	633	695
9.77–10.27	11.6–12.6	293	208
	12.6–13.6	495	482
	13.6–14.6	459	452
10.27–10.77	11.6–12.6	65	61
	12.6–13.6	280	253
	13.6–14.6	307	292

analyse the repercussion of these small differences in forthcoming sections.

4.2.2 *Radial distribution of satellites*

Fig. 6 shows the spherically averaged number density profiles of satellite galaxies with $8.77 < \log_{10} M_{star}[M_\odot] < 10.77$, normalized to the mean number density within r_{200}. We show results for galaxies inside haloes in three DMO halo mass bins, as indicated by the legend. The data points represent the profiles measured using EAGLE galaxies, whereas coloured lines display the stacked results for SHAM galaxies. For comparison, we also plot the best-fitting NFW profile to the EAGLE data, which appears to be a good description over the range of scales probed.

Given the statistical uncertainties, the number density profiles of EAGLE and SHAM galaxies agree reasonably well with the exception of V_{max}. For V_{max}, the differences are greater, it predicts shallower profiles and a lack of objects in the inner parts compared to EAGLE. This is consistent with the effects described previously: the inner parts of haloes experience large tides and are also populated by the oldest subhaloes. In contrast, on scales $r > 0.1$ Mpc, the V_{peak}, V_{infall} and V_{relax} profiles are consistent with the measurements from EAGLE for all three halo mass bins.

4.3 Galaxy clustering

We are now in the position to investigate the performance of SHAM in predicting the clustering of galaxies. We first discuss the two-point correlation function (2PCF) in real space (Section 4.3.1), then the monopole of the redshift-space correlation function (Section 4.3.2), and we end with an exploration of assembly bias in both EAGLE and SHAM (Section 4.3.3).

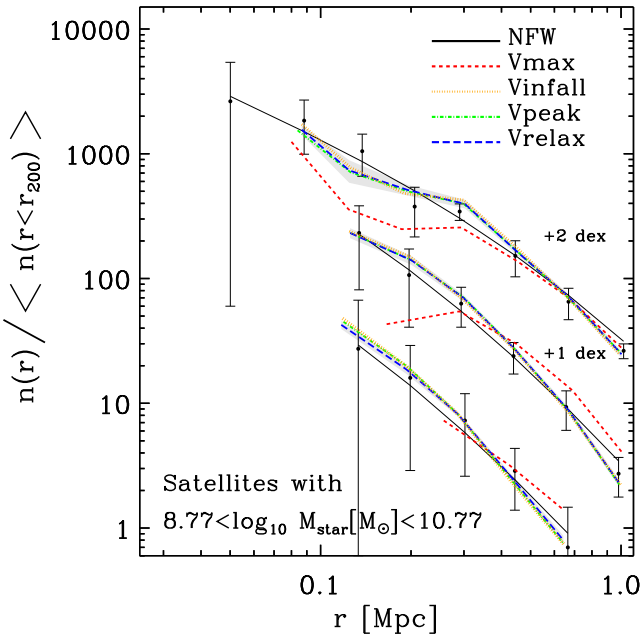

Figure 6. The radial distribution of galaxies with $8.77 < \log_{10}(M_{star}[M_\odot]) < 10.77$, inside haloes of mass $10^{13.0}$–$10^{13.5}\,M_\odot$, $10^{13.5}$–$10^{14.0}\,M_\odot$ (displaced by +1 dex), and more massive than $10^{14.0}\,M_\odot$ (displaced by +2 dex). We present the spherically averaged number density, normalized to the mean number density within the host halo. Black symbols show the results for EAGLE galaxies, whereas coloured lines show stacked results from 100 realizations of SHAM using V_{max}, V_{infall}, V_{peak}, and V_{relax}. The error bars indicate the 1σ scatter for EAGLE galaxies. The shaded region marks the standard deviation of 100 realizations of SHAM using V_{relax}. We overplot the NFW profiles (with $r_s = 0.81, 0.29, 0.21$ Mpc from the most to the least massive halo sample) that best fit the EAGLE data points shown.

We compute the 2PCF, $\xi(r)$, by Fourier transforming the galaxy number density field, which is a faster alternative to a direct pair count. We provide details of the procedure in Appendix B. We estimate the statistical uncertainties in the 2PCF of EAGLE galaxies using a spatial jackknife resampling (e.g. Zehavi et al. 2005). Summarizing, we divide the simulation box in 64 smaller boxes and then we compute 64 2PCFs removing one of the small boxes each time. The statistical errors are the standard deviation of the 64 2PCFs. On the other hand, we assign errors to the 2PCF of SHAM galaxies by computing the standard deviation of 100 realizations for each SHAM flavour.

4.3.1 *Real-space correlation function*

In Fig. 7, we compare the 2PCF for EAGLE galaxies (black solid line) with results of stacking 100 realizations of SHAM for different stellar mass bins. In the bottom panel of each subplot, we display the relative difference of the 2PCFs of each V_i galaxy sample and EAGLE ($\Delta\xi_i = \xi_i/\xi_{EAGLE} - 1$).

Fig. 7 shows that V_{max} clearly underestimates the clustering on small scales, which is consistent with the underestimation of the satellite fraction discussed earlier. A lower satellite fraction also implies a lower mean host halo mass and a smaller bias, which explains the underestimation of the correlation function on larger scales.

On the other hand, V_{infall}, V_{peak}, and V_{relax} galaxies agree very closely with the EAGLE measurements. On scales greater than

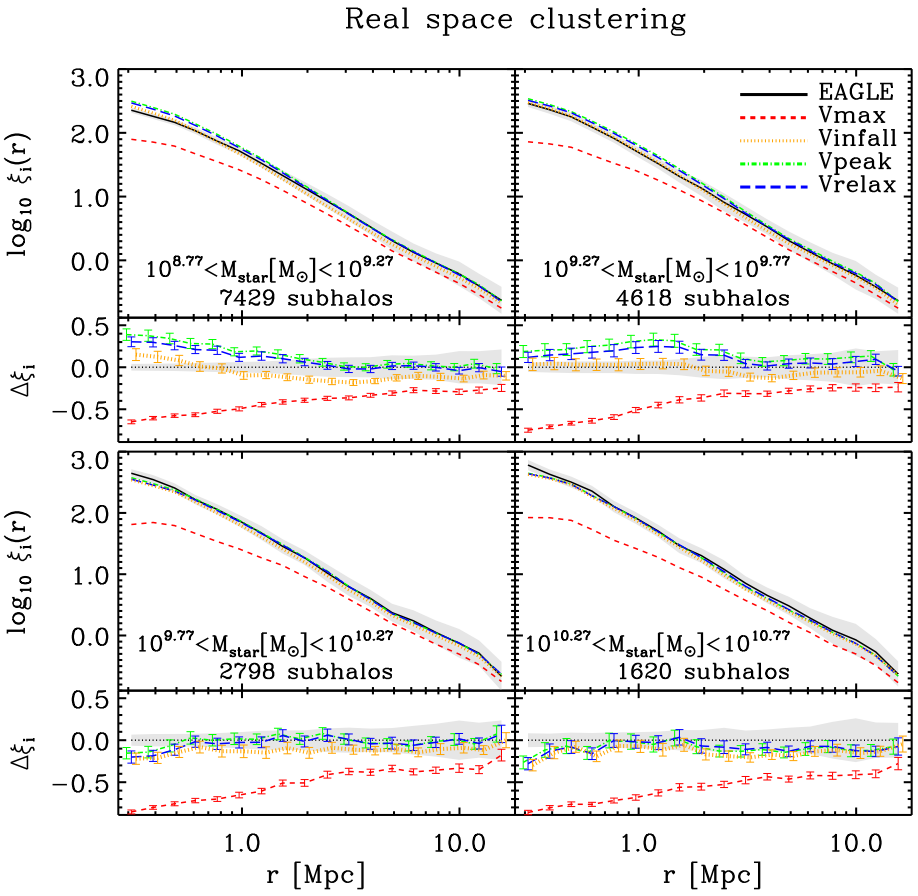

Figure 7. Real-space 2PCF for galaxies in different stellar mass bins. The black solid line shows the clustering in EAGLE, with the grey shaded region the jackknife statistical error. The coloured lines show the clustering predictions of SHAM using $V_{\rm max}$ (red dashed), $V_{\rm infall}$ (orange dotted), $V_{\rm peak}$ (green dot–dashed), and $V_{\rm relax}$ (blue long dashed). The error bars indicate the standard deviation of 100 realizations of SHAM for each flavour. In the lower half of each panel we display the relative difference of SHAM with respect to EAGLE ($\Delta\xi_i = \xi_i/\xi_{\rm EAGLE} - 1$). Note that the green and orange lines are slightly displaced horizontally for clarity. Using $V_{\rm relax}$ as SHAM parameter, we retrieve the clustering of EAGLE galaxies to within 10 per cent on scales greater than 2 Mpc.

2 Mpc, all three flavours are statistically compatible with the full hydrodynamical results. We note that the small differences are of the same order as the variance introduced by different samplings of $P(\log_{10}{\rm M_{star}}|\log_{10}V_i)$. For the two higher stellar mass bins, the statistical agreement is extended down to 400 kpc.

For the two lower stellar mass bins, we measure statistically significant differences on small scales, especially for $V_{\rm peak}$ and $V_{\rm relax}$ galaxies. The SHAM clustering appears to be 20–30 per cent high, which could originate from either more concentrated SHAM galaxy distributions inside haloes, or from an excess of satellite galaxies. At first sight, the latter explanation appears to contradict our previous finding that the satellite fraction is underpredicted by SHAM. However, the small-scale clustering will be dominated by satellites inside very massive haloes,[4] whose number is indeed overpredicted (cf. Table 5).

Additionally, Fig. 5 showed that $V_{\rm infall}$ resulted in the same underestimation of the overall satellite fraction as $V_{\rm peak}$ and $V_{\rm relax}$ but a somewhat smaller satellite fraction in the high halo mass range. This explains the weaker small-scale clustering seen in Fig. 7 and consequently the slightly better agreement with EAGLE. Note, however, that the smaller number of satellites could be caused by the fact that $V_{\rm circ}$ decreases even before accretion, especially near very massive haloes. This suggests that the apparent improved performance of $V_{\rm infall}$ could be simply a coincidence. We will investigate these hypotheses in Section 5.

[4] For instance, in the case of the small-scale clustering of galaxies in the lowest stellar mass bin, the contribution of satellites inside haloes with $M_{200} > 10^{13}\,{\rm M}_\odot$ is almost an order of magnitude larger than that of satellites in haloes with $M_{200} < 10^{13}\,{\rm M}_\odot$.

4.3.2 *Redshift-space correlation function*

Fig. 8 is analogous to Fig. 7 but for the redshift-space 2PCFs. We compute 2PCF in redshift space because they are more directly comparable with observations than the 2PCF in real space. We transform real- to redshift-space coordinates ($\boldsymbol{r}$ and $\boldsymbol{s}$, respectively) in the plane–parallel approximation: $\boldsymbol{s} = \boldsymbol{r} + (1+z)(\boldsymbol{v}\cdot\hat{\boldsymbol{k}})/H(z)$, where $\boldsymbol{v}$ the peculiar velocity, $H(z)$ is the Hubble parameter at redshift z, and $\hat{\boldsymbol{k}}$ is the unit vector along the z direction. On scales greater than 6 Mpc, this transformation enhances the clustering signal due to the Kaiser effect (Kaiser 1987). On smaller scales, motions inside virialized structures produce the so-called finger-of-god effect, smoothing the correlation function.

The differences between the SHAM flavours are qualitatively similar in real and redshift space: $V_{\rm max}$ underpredicts the clustering on all scales and for all $M_{\rm star}$ bins, the remaining SHAM flavours are statistically compatible with EAGLE on scales $\gtrsim$1 Mpc, and

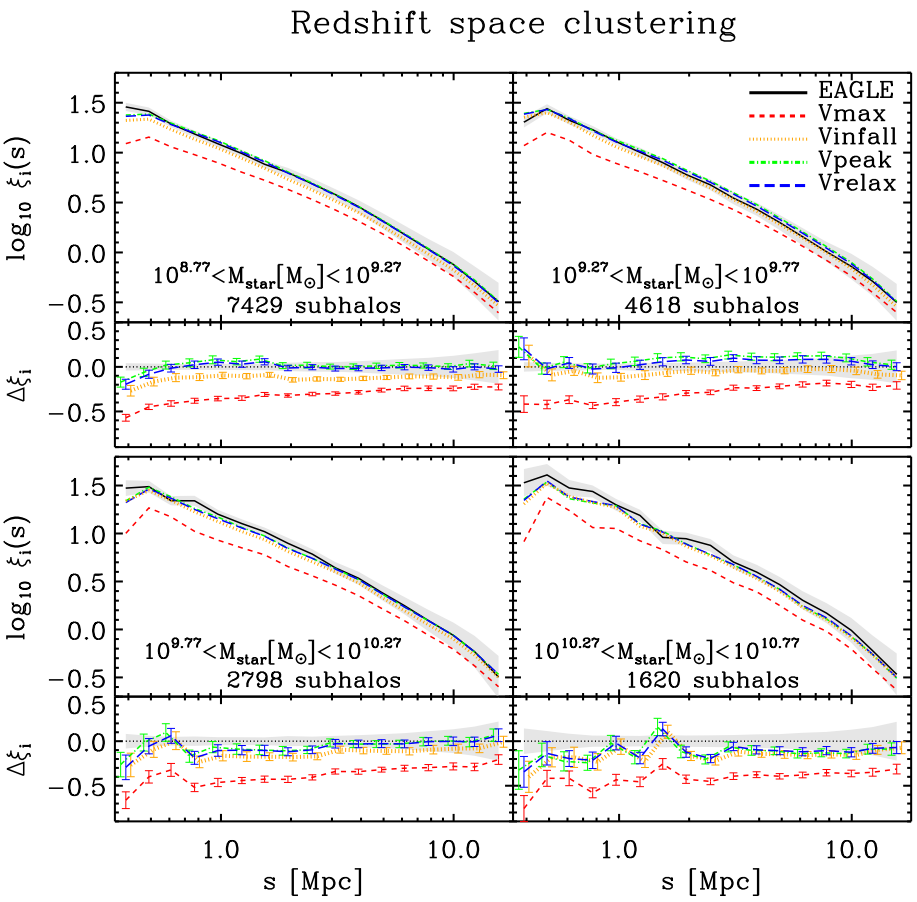

Figure 8. Same as Fig. 7 but for correlation functions computed in redshift space. The agreement between the clustering of EAGLE galaxies and V_{peak} and V_{relax} galaxies is even better in redshift space than in real space for the two lowest stellar mass bins. The main reason of the improvement on small scales is that most of the galaxies separated by those scales in redshift space are at larger distances in real space, where V_{peak} and V_{relax} galaxies accurately reproduce the clustering of EAGLE galaxies.

the clustering amplitude of V_{infall} is systematically below that of V_{relax} and V_{peak}. On the other hand, compared with the real-space 2PCFs, there is better agreement between V_{relax}, V_{peak} and EAGLE on small scales for the two lowest mass bins. This improvement is likely a result of two effects. First, a considerable fraction of close pairs in redshift space will be much further apart in real space, and hence better modelled by SHAM. Secondly, the incorrect HOD that SHAM galaxies show can be compensated by a stronger smoothing of the 2PCF: a greater number of satellites in high-mass haloes would increase the small-scale clustering, but these satellites would also have a higher velocity dispersion.

If the agreement between SHAM and EAGLE galaxies were reached because of the cancellation of different sources of error, then this would impact other orthogonal statistics, for instance, the strength of the so-called assembly bias (other examples are the high-order multipoles of the redshift space 2PCF). We explore this next.

4.3.3 Assembly bias

Assembly bias generically refers to the dependence of halo clustering on any halo property other than mass, such as formation time, concentration, or spin (see e.g. Gao et al. 2005; Gao & White 2007). It has been robustly detected in DM simulations, but it is not clear what is the effect of assembly bias on galaxy clustering. This is because a given galaxy sample will typically be a mix of haloes of different masses and properties. Although the strength of the effect depends on the assumptions of the underlying galaxy formation model, semi-analytic galaxy formation models and SHAM both suggest that assembly bias is indeed important (Croton et al. 2007; Zentner et al. 2014; Hearin et al. 2015). To our knowledge, this issue has not yet been investigated with hydrodynamical simulations.

In this section, we explore whether assembly bias is present in EAGLE and whether the different SHAM flavours are able to predict its amplitude. To quantify the effect, we will compare SHAM and EAGLE 2PCFs to those measured in shuffled galaxy catalogues, which are built following the approach of Croton et al. (2007):

(1) We compute the distance between each satellite galaxy and the COP of its host halo. This distance is by definition zero for central galaxies.

(2) We bin haloes according to M_{200} using a bin size of 0.04 dex. We verified that our results are independent of small changes in the bin widths.

(3) We randomly shuffle the entire galaxy population between haloes in the same mass bin.

(4) Finally, we assign a new position to each galaxy by moving the galaxy away from the COP of its new halo by the same distance that we calculated in (1).

Fig. 9 shows the mean relative difference between 100 realizations of the shuffled catalogues and the original for different bins of stellar mass. The black solid lines display the results for EAGLE

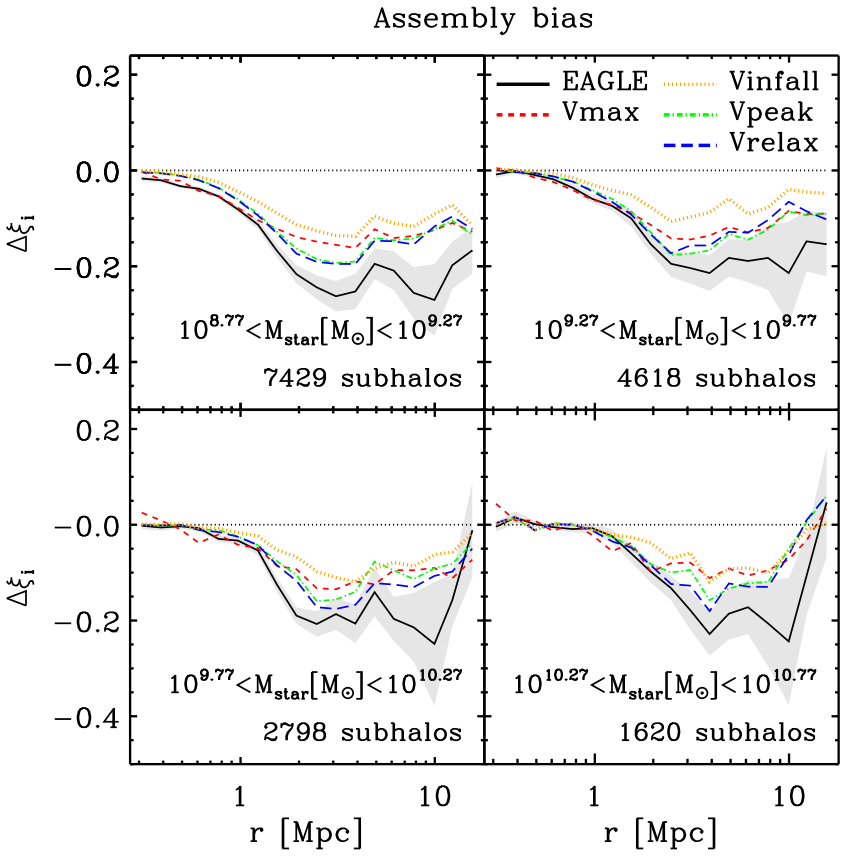

Figure 9. The relative difference of the 2PCFs of galaxies to that of a catalogue where galaxies are shuffled among haloes of the same mass ($\Delta\xi_i = \xi_i^{\rm shuff}/\xi_i^{\rm orig} - 1$, see Section 4.3.3 for more details). We adopt the same labelling as in Fig. 7. The grey shaded areas show the standard deviation after applying the shuffling procedure 100 times for EAGLE galaxies.

galaxies and the coloured lines for SHAM galaxies. Since the position of galaxies/subhaloes is independent of the environment in the shuffled catalogues, their clustering should depend exclusively on the host halo mass. Therefore, any deviations from zero in Fig. 9 can be attributed to the assembly bias. Note that on small scales the ratio goes to zero by definition since the shuffling procedure does not alter the clustering of galaxies inside the same halo.[5]

We can clearly see that all shuffled catalogues underestimate the clustering amplitude for $r \gtrsim 1$ Mpc. In the case of EAGLE galaxies, the differences are ∼20 per cent on scales greater than 2 Mpc, roughly independent of stellar mass. This implies that assembly bias increases the clustering amplitude expected from simple HOD analyses by about $1/0.8 = 25$ per cent.

For SHAM galaxies, the effect goes in the same direction but is somewhat weaker for all stellar masses (although it is more statistically significant for the lowest mass bins). This can be interpreted as SHAM lacking some environmental dependence of the relation between $M_{\rm star}$ and V_i. Likely candidates are tidal stripping of stars, and/or tidal stripping, harassment, and starvation happening before a galaxy is accreted into a larger DM halo. These effects are important because the efficiency with which a given halo creates stars will depend on the large-scale environment. We will return to these issues in the next section.

[5] Note that our findings would remain nearly the same if instead we shuffled centrals and satellites separately following Zentner et al. (2014). This is because centrals and satellites with the same $M_{\rm star}$ rarely reside in the same halo (see Fig. 5).

Before closing this section, it is interesting to note the particular case of $V_{\rm infall}$, which was the SHAM flavour that agreed best with the real-space 2PCF of EAGLE data. The fact that the strength of the assembly bias is roughly a factor of 2 smaller than in EAGLE supports the idea that the previous agreement was partly coincidental. Since $V_{\rm infall}$ will be reduced near large haloes due to interactions experimented by subhaloes before being accreted, the number of satellites will decrease and the 2PCF will decrease on small scales. However, this will likely occur for the wrong haloes, which will result in a misestimated amplitude for the assembly bias.

5 TESTING THE ASSUMPTIONS UNDERLYING SHAM

In the previous section we showed that SHAM reproduces the clustering of EAGLE galaxies to within 10 per cent on scales greater than 2 Mpc and the corresponding assembly bias reasonably well. However, small differences remain, most notably the clustering on small scales and the strength of assembly bias. In this section, we will directly test four key assumptions behind SHAM with the aim of identify the likely cause of the disagreement. Unless stated otherwise, we will employ $V_{\rm relax}$.

5.1 Assumption I: the relation between $M_{\rm star}$ and V_i is independent of redshift

One of the main assumptions in our implementation of SHAM is that $M_{\rm star}$ depends on the value of $V_{\rm relax}$, but *not* on the redshift at

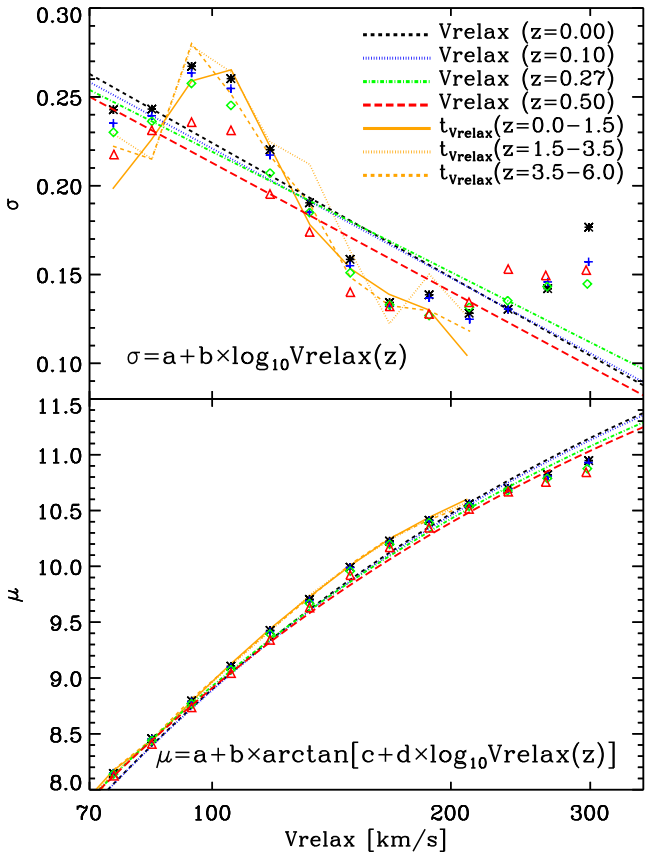

Figure 10. Standard deviation (top panel) and mean (bottom panel) of the Gaussian functions used to fit the dependence of the stellar mass PDF on $V_{\rm relax}$ at different redshifts. The symbols represent the measurements of the widths and the centres and the lines show the fits. Neither the scatter nor the mean of $M_{\rm star}$ and $V_{\rm relax}$ evolves significantly. The orange lines show the results for galaxies at $z = 0$ that have reached $V_{\rm relax}$ at $z = 0$–1.5 (solid), $z = 1.5$–3.5 (dotted), and $z = 3.5$–6 (dashed).

which $V_{\rm relax}$ was acquired. If this was not the case, we would expect an additional dependence on, for instance, the formation time of DM haloes. Such a redshift dependence would be particularly important for satellites, since on average they reach their value of $V_{\rm relax}$ at higher redshifts than centrals.

To test this assumption, we cross-matched the DMO and EAGLE catalogues at redshifts $z = [0, 0.1, 0.27,$ and $0.5]$. We do this by assuming that the link between a pair of EAGLE-DMO structures matched at $z = 0$ carries over to their main progenitors at all higher z. Then, we construct $P(\log_{10}{\rm M_{star}}|\log_{10}V_i)$ at each redshift, which we fit by Gaussian functions with mean μ and standard deviation σ. In Fig. 10 we show the results. We can see that neither the mean nor the scatter in the relation show any strong signs of redshift dependence. Nevertheless, to estimate the impact on the clustering, we generated a new set of $V_{\rm relax}$ galaxies at $z = 0$ employing the scatter and mean derived at different redshifts. We find that the differences in the 2PCF are always below 1 per cent.

As a further test, we split the $z = 0$ catalogue into three bins according to the redshift at which $V_{\rm relax}$ was reached: [0–1.5], [1.5–3.5], and [3.5–6]. We overplot the mean and variance of these subsamples in Fig. 10 as orange lines, from which we see no obvious dependence on redshift.

Therefore, we conclude that subhaloes of a given $V_{\rm relax}$ statistically host galaxies of the same $M_{\rm star}$ at $z = 0$, independently of the time at which their $V_{\rm circ}$ reached $V_{\rm relax}$.

5.2 Assumption II: baryonic physics does not affect the SHAM property of subhaloes

It is well known that baryons modify the properties of their DM hosts (Navarro, Eke & Frenk 1996; Gnedin & Zhao 2002; Read & Gilmore 2005; Oman et al. 2015). Notable examples are an increase in the central density of DM haloes due to adiabatic contraction, or the possible reduction due to feedback or episodic star formation events. However, SHAM assumes that the relevant property is that of the DM host in the absence of those baryonic effects.

We estimate the impact of this assumption by comparing the 2PCFs of central galaxies in our cross-matched catalogue, which we then rank order and select using either $V_{\rm max}$ from EAGLE or $V_{\rm max}$ from their DMO counterpart. We focus on central galaxies since $V_{\rm max}$ behaves well for those objects and should be directly relevant for $V_{\rm infall}$ satellites. In addition, the cross-matched catalogue is highly complete, with less than 8 per cent of central galaxies being excluded (see Table 2), thus we expect our results to be representative of the full population.

In general, we find that the values of $V_{\rm max}$ for EAGLE galaxies are ∼5 per cent lower than for DMO galaxies, with a scatter of 0.08 dex. However, since the scatter is 27 per cent of that of $M_{\rm star}$ at a fixed $V_{\rm max}$, we expect this difference to have only a minor effect on the clustering. This is indeed what we find. The orange dotted line in Fig. 11 shows the relative difference of the 2PCFs. The curve is compatible with zero. Note that the noise on scales below 0.5 Mpc is caused by the small number of objects at those separations owing to the absence of satellite galaxies in this analysis.

Therefore, we conclude that baryonic effects introduce only small perturbations in V_i rank ordered catalogues and will thus only have a minor effect on SHAM predictions. In any case, the noisiness of the curves do not enable us to completely rule out small changes in the galaxy clustering due to the presence of baryons.

5.3 Assumption III: baryonic physics does not affect the position of subhaloes

Another potential consequence of the presence of baryons is the modification of the positions of the subhaloes, caused by the slightly different dynamics induced by the different structure of the host halo. van Daalen et al. (2014) found this effect to be important on scales below 1 Mpc (but negligible on larger scales).

We quantify this effect by comparing the 2PCF of EAGLE galaxies in two cases; (i) using their actual positions, and (ii) using the position of their DMO counterparts. We show the relative difference between these two cases as a black solid line in Fig. 11. There are no deviations from zero on large scales and the clustering is underestimated by around 5 per cent on small scales. Therefore, the assumption that the presence of baryons does not modify the orbits of the subhaloes is justified for the range of scales explored here.

5.4 Assumption IV: for a given $V_{\rm relax}$, $M_{\rm star}$ does not depend on environment

We now address the assumption that deviations from the mean $M_{\rm star}$ at fixed $V_{\rm relax}$ are independent of the environment. Specifically, in this subsection we will investigate whether $M_{\rm star}$ at fixed $V_{\rm relax}$ is indeed uncorrelated with the host halo mass. This is a key assumption

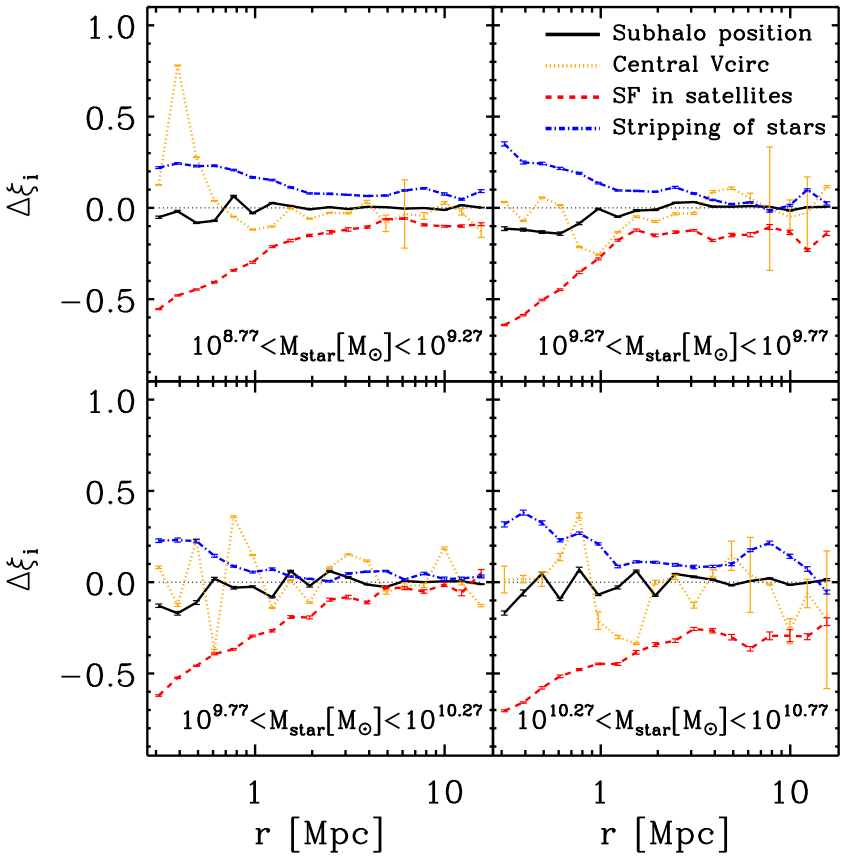

Figure 11. The impact on the 2PCF of different assumptions made by SHAM. Different lines compare the 2PCF of EAGLE with those of catalogues that aim to isolate different physical effects not included in SHAM in order to quantify their importance for modelling galaxy clustering. Black solid lines show the impact of baryonic effects on subhalo positions. Orange dotted lines show the impact of baryonic effects on $V_{\rm circ}$. Red dashed lines assess the importance of star formation in satellites after accretion. Blue dot–dashed lines show the impact of the stripping of stars inside massive haloes. The error bars display the jackknife statistical errors. See the main text for more details.

in SHAM, because it enables the modelling of galaxy clustering with a single subhalo property. Naturally, the properties of galaxies are complex functions of their merger and assembly histories, but as long as these details are not correlated with large scales, they can be treated as stochastic fluctuations within SHAM.

We start by displaying in Fig. 12 the median growth histories of central and satellite EAGLE galaxies within a narrow $V_{\rm relax}$ bin from 97 to 103 km s^{-1}. We show the evolution of $V_{\rm circ}$, $M_{\rm DM}$, $M_{\rm gas}$, and $M_{\rm star}$ for centrals (left-hand panel) and satellites (right-hand panel). Different line styles indicate the results for galaxies inside three disjoint host halo mass bins (note that the range of halo masses is different for centrals and satellites). In the case of satellites, the grey bands mark the time after these objects were accreted and brown bands mark the period after the maximum value of $M_{\rm star}(z)$ has been reached.

Interestingly, for every parameter there is a clear distinction between subhaloes hosted by haloes of different masses. Central subhaloes in the higher host halo mass bin formed more recently, host more massive galaxies, and have larger gas reservoirs than central subhaloes hosted by less massive host haloes. Centrals hosted by haloes in the most massive bin host a galaxy with a median $M_{\rm star}$ 33 per cent higher than the median value for all the subhaloes. On the other hand, centrals hosted by the least massive haloes have a median $M_{\rm star}$ 18 per cent smaller. Therefore, the difference in $M_{\rm star}$ is 0.22 dex and it corresponds to 16 per cent of the scatter in $M_{\rm star}$ at a fixed $V_{\rm relax}$ (cf. Fig. 2), which suggests that a non-negligible fraction of the scatter can be explained by host halo variations.

The evolution of satellites is also different in distinct host halo mass bins. Subhaloes that reside in more massive haloes reduce their $M_{\rm DM}$ and $V_{\rm circ}$ values more significantly, suffer from stronger stripping of gas, and stop forming stars earlier than galaxies in less massive haloes. Furthermore, these processes appear to start prior to infall in all cases (this also serves as an example of the limitation of $V_{\rm infall}$), but the earlier the higher the halo mass (see also Behroozi et al. 2014; Bahé & McCarthy 2015). Nevertheless, and contrary to the central galaxies, the final $M_{\rm star}$ is nearly independent of the host halo mass. It is also important to mention that the median $M_{\rm star}$ for satellites is 21 per cent higher than for centrals, which corresponds to 0.08 dex. Thus satellite galaxies have statistically a greater $M_{\rm star}$ than central galaxies.

In general, the evolution of satellites is more complicated than that of centrals due to processes like strangulation, harassment, ram-pressure stripping, and tidal stripping (e.g. Wetzel & White 2010; Watson et al. 2012). These effects alter the growth of satellites in a non-trivial way, which is not accounted for in SHAM. On the other hand, these processes are still not fully understood in detail, and it is not clear how realistically current hydrodynamical simulations like EAGLE capture them. For instance, a precise modelling of ram pressure necessarily requires a precise modelling of the intracluster and interstellar medium. Additionally, a precise modelling of tidal stripping requires precise morphologies of the infalling galaxies.

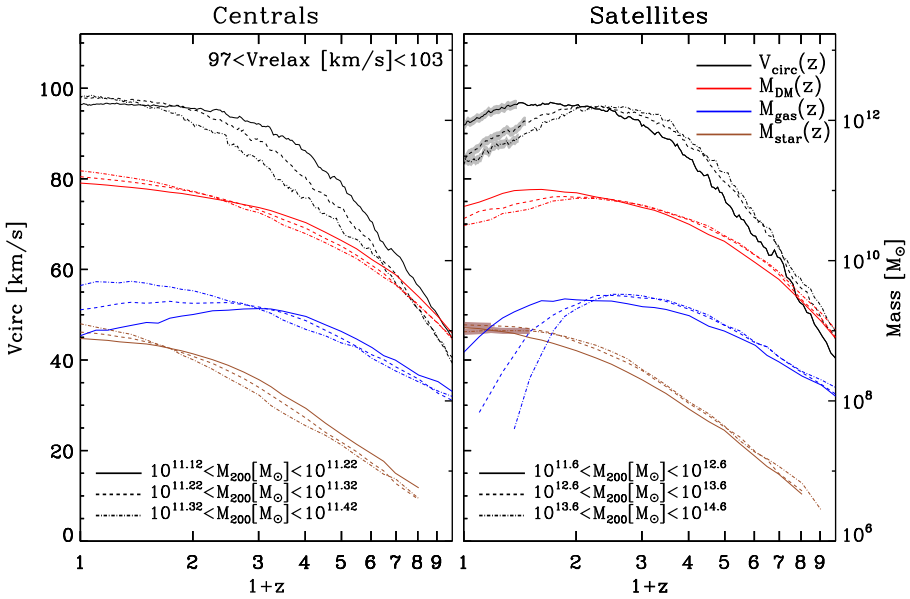

Figure 12. Evolution of the median of several subhalo properties along the merger history for centrals (left-hand panel) and satellites (right-hand panel) with $V_{\rm relax}$ between 97 and 103 km s^{-1}. The coloured lines show the evolution of the $V_{\rm circ}$, $M_{\rm DM}$, $M_{\rm gas}$, and $M_{\rm star}$, as indicated by the legend. For each component, different line styles indicate different ranges of host halo mass. Black lines are surrounded with a grey coloured area after $t_{\rm infall}$ and brown lines with a brown one after $t_{M_{\rm star}^{\rm max}}$. The centrals acquire $M_{\rm star}^{\rm max}$ at $z = 0$ and the ones that reside in more massive haloes end up with higher stellar masses. For satellites the behaviour of $M_{\rm star}$ is more complex. After infall, the satellites which contain gas continue forming stars until their gas is lost, but they can lose stellar mass due to tidal stripping. The subhaloes in the right-hand panel which reside in haloes of $10^{11.6}$–$10^{12.6}$, $10^{12.6}$–$10^{13.6}$, $10^{13.6}$–$10^{14.6}$ M$_\odot$ end up with, respectively, 99, 94, 91 per cent of their $M_{\rm star}^{\rm max}$. The stripping of DM, gas, and stars is thus more efficient for satellites in more massive host haloes (see Table 6).

Table 6. Effect of the stripping of DM and stars from satellites, and of star formation after infall. Each value corresponds to the median of the distribution and its uncertainty computed as $\sigma = 1.4826\,{\rm MAD}/\sqrt{n}$, where MAD is the median absolute deviation and n the number of elements.

M_{200}[M$_\odot$]	$\frac{M_{\rm DM}}{M_{\rm DM}^{\rm max}}$	$\frac{M_{\rm star}}{M_{\rm star}^{\rm max}}$	$\frac{M_{\rm star}}{M_{\rm star}^{\rm infall}}$
	$M_{\rm star} = 10^{8.77}$–$10^{9.27}$M$_\odot$		
$10^{11.6}$–$10^{12.6}$	0.428 ± 0.011	1.000 ± 0.000	1.714 ± 0.030
$10^{12.6}$–$10^{13.6}$	0.314 ± 0.008	0.954 ± 0.002	1.828 ± 0.035
$10^{13.6}$–$10^{14.6}$	0.274 ± 0.008	0.904 ± 0.004	1.446 ± 0.024
	$M_{\rm star} = 10^{9.27}$–$10^{9.77}$ M$_\odot$		
$10^{11.6}$–$10^{12.6}$	0.458 ± 0.015	1.000 ± 0.000	1.526 ± 0.028
$10^{12.6}$–$10^{13.6}$	0.329 ± 0.011	0.987 ± 0.001	1.752 ± 0.037
$10^{13.6}$–$10^{14.6}$	0.278 ± 0.011	0.935 ± 0.004	1.550 ± 0.034
	$M_{\rm star} = 10^{9.77}$–$10^{10.27}$ M$_\odot$		
$10^{11.6}$–$10^{12.6}$	0.489 ± 0.023	1.000 ± 0.000	1.360 ± 0.027
$10^{12.6}$–$10^{13.6}$	0.352 ± 0.014	0.998 ± 0.000	1.532 ± 0.033
$10^{13.6}$–$10^{14.6}$	0.263 ± 0.012	0.945 ± 0.004	1.433 ± 0.030
	$M_{\rm star} = 10^{10.27}$–$10^{10.77}$ M$_\odot$		
$10^{11.6}$–$10^{12.6}$	0.670 ± 0.049	1.000 ± 0.000	1.187 ± 0.032
$10^{12.6}$–$10^{13.6}$	0.386 ± 0.020	0.993 ± 0.001	1.197 ± 0.018
$10^{13.6}$–$10^{14.6}$	0.238 ± 0.014	0.937 ± 0.005	1.246 ± 0.025

Hence, we choose to bracket their impact on SHAM clustering predictions by considering two extreme situations.

We first consider a situation where satellite galaxies do not form or lose any stars after infall, i.e. the value of $M_{\rm star}$ is fixed at infall. The last column in Table 6 compares $M_{\rm star}$ at infall with $M_{\rm star}$ at $z = 0$ for galaxies hosted by haloes of different masses. The corresponding relative difference in the 2PCF is displayed by a red line in Fig. 11. In this case the satellites are less massive, which causes SHAM to result in a 10–20 per cent (depending on the range of $M_{\rm star}$ considered) lower clustering signal on large scales. On small scales, the deficiency is larger, reaching more than 50 per cent.

The second situation we consider is one where there is no tidal stripping of stars in satellite galaxies, i.e. performing SHAM using the maximum value of $M_{\rm star}$ a galaxy has ever attained along its history, $M_{\rm star}^{\rm max}$. In Table 6, we compare the values of $M_{\rm star}^{\rm max}$ with $M_{\rm star}$ at $z = 0$ for different bins in stellar and host halo mass. On average, we find that the $M_{\rm star}$ reduction begins after satellites have lost about 2/3 of their $M_{\rm DM}$. We also find that this effect is stronger for low-mass galaxies in higher mass haloes, which is indeed expected due to the stronger tides. The reduction can be up to 10 per cent in haloes with $M_{200} > 10^{13.6}$ M$_\odot$. On the other hand, this effect is essentially zero in haloes with $M_{200} < 10^{12.6}$ M$_\odot$.

To quantify how the stripping of stars affects the SHAM clustering predictions, we calculate the 2PCF after selecting galaxies according to $M_{\rm star}^{\rm max}$ and compare it to our fiducial EAGLE catalogue. The result is shown by the blue dot–dashed lines in Fig. 11. In this case, the clustering is enhanced by about 10 per cent on scales greater than 1 Mpc and by up to 35 per cent on scales below 1 Mpc. This can be understood from the fact that the satellites are more massive, causing the satellite fraction and mean host halo mass increase, which affects the 2PCF particularly on small scales.

The two effects considered here, stellar stripping and reduced gas supply in satellites, affect the SHAM galaxy clustering to a similar magnitude but with opposite sign. In particular, for all $M_{\rm star}$ their impact is larger than the differences between SHAM and EAGLE predictions. Thus, the final galaxy clustering is sensitive to how these processes balance each other, which in turn depends sensitively on baryonic processes not yet fully understood quantitatively. On the one hand, this implies an intrinsic limitation of current SHAM modelling that is reached when better than ∼20 per cent accuracy

is required. On the other hand, this suggests that galaxy clustering on small scales is a powerful test for the physics implemented in hydrodynamical simulations. For instance, if SHAM results were to be taken as the reality and confirmed by observations, then EAGLE would implement too weak ram-pressure stripping of massive satellite galaxies and excessive stellar stripping of low-mass galaxies in haloes with $M_{200} > 10^{12.6}\,\mathrm{M}_\odot$.

6 CONCLUSIONS

We have used the Ref-L100N1504 EAGLE cosmological hydrodynamical simulation to perform a detailed analysis of SHAM for galaxies with stellar mass ranging from $10^{8.77}\,\mathrm{M}_\odot$ to $10^{10.77}\,\mathrm{M}_\odot$. We used a catalogue of paired EAGLE galaxies and subhaloes in a corresponding DM-only simulation to search for an optimal implementation of SHAM, to test its performance in terms of halo occupation numbers, radial number density profiles, galaxy clustering, and assembly bias, and to investigate the validity of some of the key assumptions underlying SHAM.

Our main findings can be summarized as follows.

(i) We argue that all current SHAM implementations use DM properties that are affected by undesired physical or numerical artefacts. Thus, we propose a new measure: $V_{\rm relax}$, which is defined as the maximum circular velocity that a subhalo has reached while satisfying a relaxation criterion. We also studied SHAM using three other subhalo properties: $V_{\rm max}$, the maximum circular velocity at $z = 0$; $V_{\rm infall}$, the maximum circular velocity at the last time a subhalo was a central; and $V_{\rm peak}$, the maximum circular velocity that a subhalo has reached. In Fig. 4 we show that out of the four SHAM flavours we tested, $V_{\rm relax}$ exhibits the strongest correlation with $M_{\rm star}$, independently of the subhalo history.

(ii) $V_{\rm infall}$, $V_{\rm peak}$, and $V_{\rm relax}$ reproduce the EAGLE predictions reasonably well (with $V_{\rm relax}$ performing slightly better than $V_{\rm infall}$ and $V_{\rm peak}$):

(a) Fig. 5 shows that the distributions of host halo masses between EAGLE and SHAM flavours match closely. In particular, the total satellite galaxy fraction agrees to within 5 per cent.

(b) Fig. 7 shows that galaxy clustering strength agrees to within 10 per cent on scales greater than 1 Mpc and within 30 per cent on smaller scales. We highlight that this relation holds over four orders of magnitude in amplitude and three in length scale.

(c) Fig. 8 shows that in redshift space the agreement improves to the point that there is no statistically significant discrepancy.

(d) Assembly bias is present both in EAGLE and in its SHAM catalogues. Fig. 9 shows that assembly bias increases the clustering by about 20 per cent.

Although small, the differences between EAGLE and SHAM are systematic and significant. We attribute these to SHAM slightly overpredicting, compared to EAGLE galaxies, the fraction of low-mass satellites in massive haloes.

(iii) Fig. 12 shows that there is a relation between $M_{\rm star}$ and halo mass at fixed $V_{\rm relax}$. Centrals hosted by more massive haloes typically have higher $M_{\rm star}$, formed more recently, and contain more gas than those hosted by smaller haloes. Satellites that reside in more massive haloes typically reduce their $M_{\rm DM}$ and $V_{\rm circ}$ values more significantly, suffer from stronger stripping of gas, and stop forming stars before accretion and earlier than those in less massive haloes. The $M_{\rm star}$ of satellite galaxies at $z = 0$ is independent of the host halo mass and it is $\sim$20 per cent greater than the $M_{\rm star}$ of central galaxies at fixed $V_{\rm relax}$.

(iv) Interactions between satellites and their host haloes are very important for the amplitude of the correlation function, especially on small scales. We show in Fig. 11 that the difference between two extreme cases: where no stars are formed after accretion and where galaxies suffer no stripping of stars, result in differences in the amplitude of the 2PCF of $\pm$20 per cent on large scales and almost a factor of 2 on small scales.

We note that, although the box size of EAGLE (100 Mpc) is among the largest for simulations of its type, it is not large enough to ensure converged clustering properties. The lack of long wavemodes produces a few per cent excess of haloes with $M \lesssim 10^{14}\,\mathrm{M}_\odot$ and a larger deficiency of more massive haloes. We expect this to reduce the satellite fraction, which may affect the shape and amplitude of overall correlation function, and might thus make our assessment of SHAM slightly too optimistic.

Overall, our results confirm the usefulness of SHAM for interpreting and modelling galaxy clustering. However, they also highlight the limits of current SHAM implementations when an accuracy better than $\sim$20 per cent is required. Beyond this point, details of galaxy formation physics become important. For instance, SHAM assumes that the relation between $V_{\rm relax}$ and $M_{\rm star}$ is independent of the host halo mass. However, the validity of this assumption depends on how efficiently the gas content of satellite galaxies is depleted after accretion, on the importance of the stripping of stars in different environments, and on the relation between $M_{\rm DM}$ and $M_{\rm star}$ for centrals. EAGLE suggests that these effects depend on the host halo mass (and thus possibly on cosmological parameters), which would break the family of one-parameter SHAM models.

Fortunately, it seems possible that these physical processes can be modelled, and marginalized over, within SHAM. An interesting line of development would be the extension of SHAM to a two-parameter model, for instance a function of $V_{\rm relax}$ and $M_{\rm halo}$. This would not only reduce the systematic biases in the correlation function, but would also increase the predictive power of SHAM for centrals. We plan to explore this in the future.

Naturally, as hydrodynamical simulations improve their realism, it should be possible to better model the evolution of galaxies hosted by massive clusters, which will lead to more accurate SHAM implementations and a more accurate assessment of its performance. Ultimately, these developments will enable quick and precise predictions for the clustering of galaxies in the highly non-linear regime. In principle, this could be extended as a function of cosmology employing, e.g. cosmology-scaling methods (Angulo & White 2010; Angulo & Hilbert 2015). This opens up many interesting possibilities, such as the direct use of SHAM to optimally exploit the overwhelmingly rich and accurate clustering measurements that are expected to arrive over the next decade.

ACKNOWLEDGEMENTS

We would like to thank Oliver Hahn and Peter Behroozi for useful discussions. Most of the parameters for EAGLE galaxies are available from the data base (McAlpine+) or through interaction with the authors. This research was supported in part by the European Research Council under the European Union's Seventh Framework Programme (FP7/2007-2013)/ERC Grant agreement 278594-GasAroundGalaxies, GA 267291 Cosmiway, and 321334 dustygal, the Interuniversity Attraction Poles Programme initiated by the Belgian Science Policy Office [AP P7/08 CHARM]. This work used the DiRAC Data Centric system at Durham University, operated by the Institute for Computational Cosmology on

behalf of the STFC DiRAC HPC Facility (www.dirac.ac.uk). This equipment was funded by BIS National E-infrastructure capital grant ST/K00042X/1, STFC capital grant ST/H008519/1, and STFC DiRAC Operations grant ST/K003267/1 and Durham University. DiRAC is part of the National E-Infrastructure. JCM acknowledges support from the Fundación Bancaria Ibercaja for developing this research.

REFERENCES

Angulo R. E., Hilbert S., 2015, MNRAS, 448, 364
Angulo R. E., White S. D. M., 2010, MNRAS, 405, 143
Angulo R. E., Baugh C. M., Frenk C. S., Lacey C. G., 2008, MNRAS, 383, 755
Angulo R. E., Lacey C. G., Baugh C. M., Frenk C. S., 2009, MNRAS, 399, 983
Bahé Y. M., McCarthy I. G., 2015, MNRAS, 447, 969
Bahé Y. M., McCarthy I. G., Balogh M. L., Font A. S., 2013, MNRAS, 430, 3017
Behroozi P. S., Conroy C., Wechsler R. H., 2010, ApJ, 717, 379
Behroozi P. S., Wechsler R. H., Lu Y., Hahn O., Busha M. T., Klypin A., Primack J. R., 2014, ApJ, 787, 156
Conroy C., Wechsler R. H., Kravtsov A. V., 2006, ApJ, 647, 201
Contreras S., Baugh C. M., Norberg P., Padilla N., 2015, MNRAS, 452, 1861
Crain R. A. et al., 2015, MNRAS, 450, 1937
Croton D. J., Gao L., White S. D. M., 2007, MNRAS, 374, 1303
Dalal N., White M., Bond J. R., Shirokov A., 2008, ApJ, 687, 12
Dalla Vecchia C., Schaye J., 2012, MNRAS, 426, 140
Davis M., Efstathiou G., Frenk C. S., White S. D. M., 1985, ApJ, 292, 371
Dolag K., Borgani S., Murante G., Springel V., 2009, MNRAS, 399, 497
Durier F., Dalla Vecchia C., 2012, MNRAS, 419, 465
Gao L., White S. D. M., 2007, MNRAS, 377, L5
Gao L., Springel V., White S. D. M., 2005, MNRAS, 363, L66
Gnedin O. Y., 2003, ApJ, 582, 141
Gnedin O. Y., Zhao H., 2002, MNRAS, 333, 299
Guo Q., White S., Li C., Boylan-Kolchin M., 2010, MNRAS, 404, 1111
Hayashi E., Navarro J. F., Taylor J. E., Stadel J., Quinn T., 2003, ApJ, 584, 541
Hearin A. P., Watson D. F., van den Bosch F. C., 2015, MNRAS, 452, 1958
Hopkins P. F., 2013, MNRAS, 428, 2840
Jiang L., Helly J. C., Cole S., Frenk C. S., 2014, MNRAS, 440, 2115
Kaiser N., 1987, MNRAS, 227, 1
Kravtsov A. V., Gnedin O. Y., Klypin A. A., 2004, ApJ, 609, 482
Kuhlen M., Vogelsberger M., Angulo R., 2012, Phys. Dark Universe, 1, 50
Lacerna I., Padilla N., 2011, MNRAS, 412, 1283
Lacerna I., Padilla N., 2012, MNRAS, 426, L26
Lacerna I., Padilla N., Stasyszyn F., 2014, MNRAS, 443, 3107
Li Y., Mo H. J., Gao L., 2008, MNRAS, 389, 1419
Ludlow A. D., Navarro J. F., Li M., Angulo R. E., Boylan-Kolchin M., Bett P. E., 2012, MNRAS, 427, 1322
Mo H. J., White S. D. M., 1996, MNRAS, 282, 347
Moster B. P., Somerville R. S., Maulbetsch C., van den Bosch F. C., Macciò A. V., Naab T., Oser L., 2010, ApJ, 710, 903
Nagai D., Kravtsov A. V., 2005, ApJ, 618, 557
Navarro J. F., Eke V. R., Frenk C. S., 1996, MNRAS, 283, L72
Neto A. F. et al., 2007, MNRAS, 381, 1450
Nuza S. E. et al., 2013, MNRAS, 432, 743
Oman K. A. et al., 2015, MNRAS, 452, 3650
Peacock J. A., Smith R. E., 2000, MNRAS, 318, 1144
Peebles P. J. E., 2001, in Martínez V. J., Trimble V., Pons-Bordería M. J., eds, ASP Conf. Ser., Vol. 252, Historical Development of Modern Cosmology. Astron. Soc. Pac., San Francisco, p. 201
Peñarrubia J., McConnachie A. W., Navarro J. F., 2008, ApJ, 672, 904
Planck Collaboration I, 2014, A&A, 571, A1
Planck Collaboration XVI, 2014, A&A, 571, A16
Read J. I., Gilmore G., 2005, MNRAS, 356, 107
Reddick R. M., Wechsler R. H., Tinker J. L., Behroozi P. S., 2013, ApJ, 771, 30
Rosas-Guevara Y. M. et al., 2013, MNRAS, 454, 1038
Schaller M. et al., 2015, MNRAS, 451, 1247
Schaye J., Dalla Vecchia C., 2008, MNRAS, 383, 1210
Schaye J. et al., 2015, MNRAS, 446, 521
Scoccimarro R., Sheth R. K., Hui L., Jain B., 2001, ApJ, 546, 20
Seljak U., 2000, MNRAS, 318, 203
Shankar F., Lapi A., Salucci P., De Zotti G., Danese L., 2006, ApJ, 643, 14
Simha V., Cole S., 2013, MNRAS, 436, 1142
Simha V., Weinberg D. H., Davé R., Fardal M., Katz N., Oppenheimer B. D., 2012, MNRAS, 423, 3458
Springel V., 2005, MNRAS, 364, 1105
Springel V., White S. D. M., Tormen G., Kauffmann G., 2001, MNRAS, 328, 726
Trujillo-Gomez S., Klypin A., Primack J., Romanowsky A. J., 2011, ApJ, 742, 16
Vale A., Ostriker J. P., 2004, MNRAS, 353, 189
van Daalen M. P., Schaye J., McCarthy I. G., Booth C. M., Dalla Vecchia C., 2014, MNRAS, 440, 2997
Velliscig M., van Daalen M. P., Schaye J., McCarthy I. G., Cacciato M., Le Brun A. M. C., Dalla Vecchia C., 2014, MNRAS, 442, 2641
Vogelsberger M. et al., 2014, MNRAS, 444, 1518
Watson D. F., Berlind A. A., Zentner A. R., 2012, ApJ, 754, 90
Wechsler R. H., Zentner A. R., Bullock J. S., Kravtsov A. V., Allgood B., 2006, ApJ, 652, 71
Weinberg D. H., Colombi S., Davé R., Katz N., 2008, ApJ, 678, 6
Wetzel A. R., White M., 2010, MNRAS, 403, 1072
Wetzel A. R., Cohn J. D., White M., 2009, MNRAS, 395, 1376
Wetzel A. R., Tinker J. L., Conroy C., van den Bosch F. C., 2013, MNRAS, 432, 336
Wetzel A. R., Tinker J. L., Conroy C., van den Bosch F. C., 2014, MNRAS, 439, 2687
Wiersma R. P. C., Schaye J., Smith B. D., 2009a, MNRAS, 393, 99
Wiersma R. P. C., Schaye J., Theuns T., Dalla Vecchia C., Tornatore L., 2009b, MNRAS, 399, 574
Zehavi I. et al., 2005, ApJ, 630, 1
Zentner A. R., Hearin A. P., van den Bosch F. C., 2014, MNRAS, 443, 3044
Zhu G., Zheng Z., Lin W. P., Jing Y. P., Kang X., Gao L., 2006, ApJ, 639, L5
Zu Y., Zheng Z., Zhu G., Jing Y. P., 2008, ApJ, 686, 41

APPENDIX A: RESOLUTION

In this section, we will present two tests that suggest that our results are not affected by the finite mass and force resolution of the EAGLE and DMO simulations. Specifically, we will explore the number of DM particles of the SHAM galaxies and compare simulations with different resolutions.

In Fig. A1 we show the PDF of the number of DM particles associated with central (top panel) and satellite (bottom panel) SHAM galaxies. Coloured lines show the results for different $M_{\rm star}$ bins using $V_{\rm relax}$. The detection threshold of our SUBFIND catalogues (20 particles) is marked by a vertical dashed line. The top panel shows that nearly all the central subhaloes are resolved more than 1000 DM particles. Satellites, on the other hand, are resolved with fewer particles because some of them will be lost to tidal stripping. However, since the value of $V_{\rm relax}$ will be acquired before the stripping begins, we do not expect this to affect our results. The only effect that might be important is that a subhalo can fall below the detection threshold while its counterpart galaxy is still resolved. We see that this might be the case for a very small fraction subhaloes in the lowest $M_{\rm star}$ bin. We quantify these effects next.

In Fig. A2, we show the number density of satellites (top panel) and the satellite fraction (bottom panel) for three different EAGLE

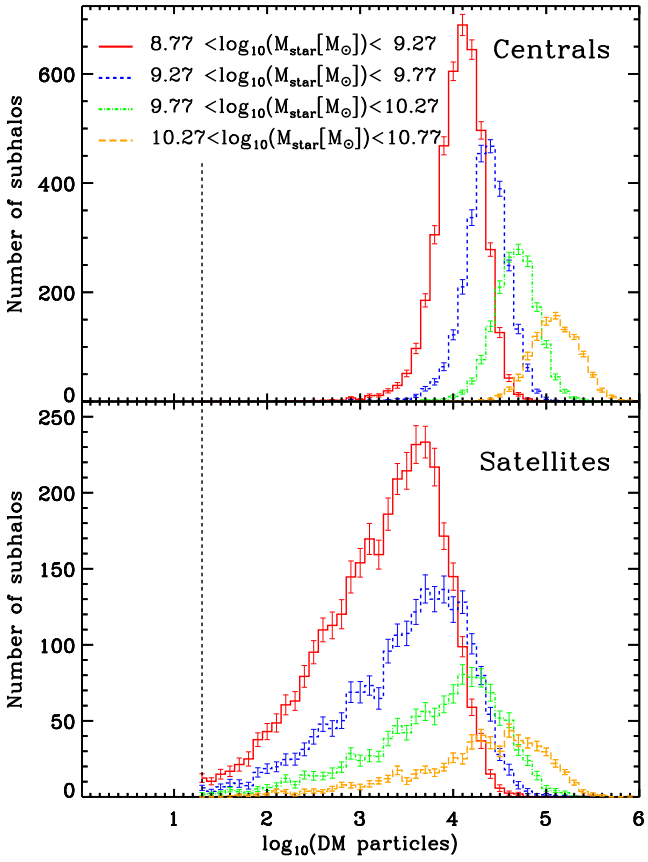

Figure A1. Number of DM particles in subhaloes of a given $M_{\rm star}$. The coloured lines represent the mean PDFs of 100 realizations using $V_{\rm relax}$ for different stellar mass bins and the errors are the standard deviation of the 100 realizations. The top (bottom) panel shows the PDFs of centrals (satellites). The black dashed line indicates the detection threshold of our SUBFIND catalogues. The centrals are always resolved with more than 1000 particles. However, the satellites have a tail in their distribution which reaches the detection threshold.

simulations and their DMO counterparts. The black lines show the results for the same simulation used in this paper (Ref-L100N1504), the blue lines for a simulation with 25 Mpc on a side and the same resolution as Ref-L100N1504 (Ref-L025N376), and the red lines for a simulation with 25 Mpc on a side and eight times higher mass resolution than Ref-L100N1504 (Ref-L025N752). To estimate the cosmic variance, we divide Ref-L100N1504 into 64 boxes of 25 Mpc on a side; the grey shaded areas enclose the 68 per cent of these boxes. The regions enclosed by vertical dotted lines in the bottom panels indicate the bins employed in Section 4.

The left two panels show that galaxies according to $M_{\rm star}$ or $V_{\rm max}$ produce almost identical satellite fractions in both (Ref-L025N752) and (Ref-L025N386), despite the former having eight times better mass resolution. The satellite fraction coincides with our main EAGLE run for high number densities, but underpredicts the satellite fraction at low number densities. This, however, is plausibly explained by cosmic variance and the lack of long wave modes due to the smaller volume (64 times). The rightmost panel shows the DMO versions, for which the agreement between different resolutions is even better. Thus, this suggests that the results presented in this paper are not affected by the numerical resolution of our simulations.

APPENDIX B: CORRELATION FUNCTION CALCULATION

The 2PCF counts the number of pairs at different distances in relation to the number of pairs that one would have expected from a random distribution (see e.g. Davis et al. 1985; Peebles 2001):

$$\mathrm{d}P = n^2[1 + \xi(\boldsymbol{r}_{12})]\mathrm{d}V_1 dV_2, \tag{B1}$$

where n is the mean density and $\xi(\boldsymbol{r}_{12})$ the correlation function. This equation describes the excess probability, compared with a random sample, of finding a point in an element of volume $\mathrm{d}V_2$ at a distance $\boldsymbol{r}_{12}$ from another point in $\mathrm{d}V_1$. The 2PCF is also the Fourier

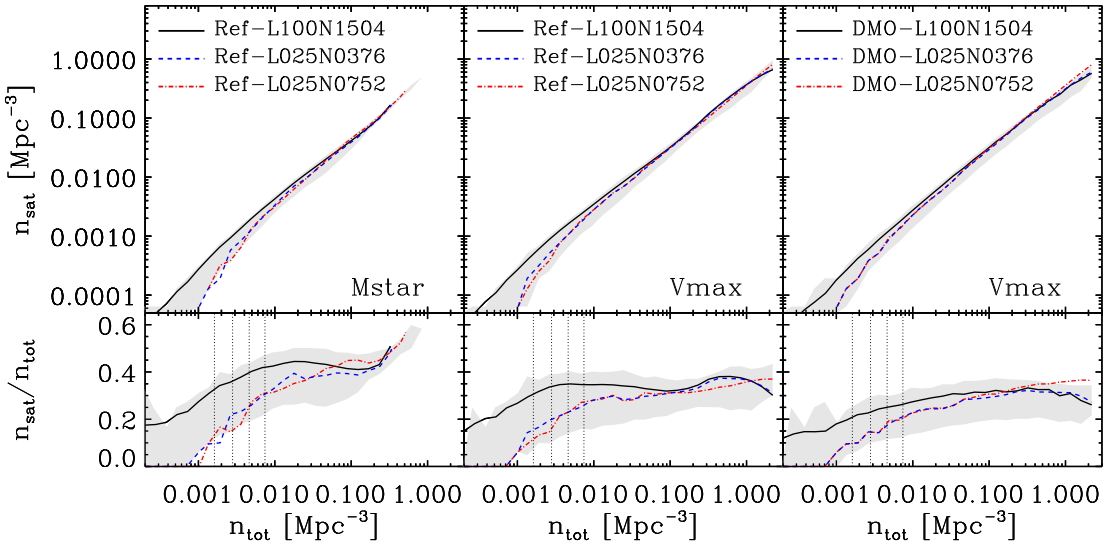

Figure A2. Number density of satellites (top panels) and satellite fraction (bottom panels) versus total number density. In the left-hand, centre, and right-hand panels subhaloes are ordered according to $M_{\rm star}^{\rm Ref}$, $V_{\rm max}^{\rm Ref}$, and $V_{\rm max}^{\rm DMO}$, respectively. Coloured lines show the results for different simulations. The grey shaded areas enclose the 68 per cent of the results after dividing the simulation with the largest volume into 64 smaller boxes of 25 Mpc on a side. The regions enclosed by dotted lines indicate the bins employed in Section 4.

transform (FT) of the power spectrum $P(\boldsymbol{k})$:

$$\xi(\boldsymbol{r}) = \frac{1}{(2\pi)^3}\int \mathrm{d}k^3 P(\boldsymbol{k})\mathrm{e}^{\mathrm{i}\boldsymbol{k}\cdot\boldsymbol{x}}, \tag{B2}$$

and the power spectrum is defined as

$$\left\langle \hat{\delta}(\boldsymbol{k})\hat{\delta}(\boldsymbol{k}')\right\rangle = (2\pi)^3\delta_{\mathrm{D}}(\boldsymbol{k}-\boldsymbol{k}')P(\boldsymbol{k}), \tag{B3}$$

where $\hat{\delta}(\boldsymbol{k})$ is the FT of the density contrast and $\delta_{\mathrm{D}}(\boldsymbol{k})$ is the Dirac delta function. We can use this property to quickly compute the 2PCF using the fast FT. To calculate the 2PCF, we follow the following steps.

(i) We divide the simulation cube into 1024^3 boxes of 97.6 kpc on a side. We determine in each box the density contrast using a cloud-in-cell scheme. The density contrast is defined as

$$\delta(\boldsymbol{x}) = \frac{N-\langle N\rangle}{\langle N\rangle}, \tag{B4}$$

where N is the number of subhaloes inside one box and $\langle N\rangle$ is the total number of subhaloes in the simulation cube.

(ii) The FT of the density field is

$$\hat{\delta}(\boldsymbol{k}) = \int \mathrm{d}x^3\mathrm{e}^{-\mathrm{i}\boldsymbol{k}\cdot\boldsymbol{x}}\delta(\boldsymbol{x}), \tag{B5}$$

we compute this FT using version 3.3.3 of the Fastest Fourier Transform in the West (FFTW3; http://www.fftw.org/), a compilation of C routines for computing the discrete FT.

(iii) We calculate $P(\boldsymbol{k})$ using equation (B3) and then we subtract the Poisson noise. The Poisson noise arises from sampling a continuous distribution with a discrete number of objects. It scales as $1/n$, where n is the number density of objects.

(iv) The next step is to go back to real space by computing the FT of $P(\boldsymbol{k})$, yielding the 2PCF.

(v) Finally, we spherically average the correlation function obtaining the 3D 2PCF $\xi(|\boldsymbol{r}|)$.

By dividing the simulation cube into different number of cells, we verified that using 1024^3 boxes represents the clustering beyond 0.3 Mpc faithfully.

This paper has been typeset from a TEX/LATEX file prepared by the author.